Source Distribution Analysis of Magnetic Microscopy Maps of Geological Samples

by

Joseph B. Silverman

Submitted to the Department of Mechanical Engineering

in Partial Fulfillment of the Requirements for the Degree of

Bachelor of Science in Mechanical Engineering with a concentration in Space Systems Engineering

at the Massachusetts Institute of Technology

May 17, 2010
[June 2010]

Author_____
Joseph B. Silverman
Department of Mechanical Engineering

Certified by_____
Research Scientist Eduardo A. Lima
Thesis Supervisor

Certified_____
Professor Benjamin P. Weiss
Thesis Supervisor

Certified by_____
Professor Kamal Youcef-Toumi
Thesis Supervisor

Accepted by_____
John H. Lienhard V
Collins Professor of Mechanical Engineering
Chairman, Undergraduate Thesis Committee

Source Distribution Analysis of Magnetic Microscopy Maps of Geological Samples

by

Joseph B. Silverman

Submitted to the Department of Mechanical Engineering
on May 17, 2010 in Partial Fulfillment of the Requirements for the
Degree of Bachelor of Science in Mechanical Engineering with a
concentration in Space Systems Engineering

Abstract

Superconducting quantum interference devices (SQUID) are currently the most sensitive magnetometers for geological samples. Standard SQUID magnetometers are able to directly estimate the net moment of a sample, while SQUID microscopes require complex inversion of maps of the magnetic field above the sample. In order to extract magnetization information from SQUID microscope measurements, it is customary to model the sample as a distribution of magnetic dipoles. The calculations required for this operation in the space domain typically involve a pseudoinversion which becomes problematic due to the large amount of data, measurement noise, inherent loss of information in computational discretization, and ambiguity in determining an optimized "best" solution. To ameliorate these problems, we have implemented several regularization techniques and constraints. Using synthetic, computationally generated measurements, our investigation demonstrates that Tikhonov regularization with a high-pass filter matrix performs better than unregularized least square methods, truncated singular value decomposition, and Tikhonov regularization using an identity matrix (minimum norm). Our study also gives insight regarding the benefit and cost of setting various constraints. Our findings are then tested on real measurements of a sample of shocked basalt and a test sample comprised of a section of a refrigerator magnet.

Direct Supervisor: Dr. Eduardo A. Lima
Title: Research Scientist for the Department of Earth Atmospheric and Planetary Science

Faculty Advisor: Professor Benjamin P. Weiss
Title: Associate Professor of Earth Atmospheric and Planetary Science

Thesis Advisor: Professor Kamal Youcef-Toumi
Title: Professor of Mechanical Engineering

Table of Contents

List of Tables

List of Tables

1. Introduction

From studying the remnant magnetic field of minerals and rocks it is possible to make broad statements about the magnetic conditions of the environment where they formed initially as well as the magnetic conditions the sample has been subjected to since formation (Butler, 2004). This area of research is called paleomagnetism and it is often used to describe the history of the magnetic field of earth and other planetary bodies (Weiss, Lima, Fong, & Baudenbacher, 2007), (Gattacceca, Berthe, Boustie, Vadeboin, Rochette, & de Resseguier, 2008), (Weiss, Fong, Vali, Lima, & Baudenbacher, 2008). It was also instrumental in developing the theory of continental drift (Butler, 2004). As instrumentation for this field advances to measure weaker magnetic fields with better spatial resolution, a wider variety of minerals and rocks can be studied in greater detail than ever before providing new directions for scientific exploration.

Superconducting quantum interference devices (SQUIDs) are the state of the art magnetometers for making quantitative measurements of weak magnetic fields (Clarke & Braginski, 2004), (Jenks, Thomas, & Wikswo, 1997). Their applications range from measuring electrical impulses in organs such as the heart, to analyzing current flow in integrated circuits. SQUID moment magnetometers, which measure the net magnitude and orientation of a sample's moment, have been extensively used in paleomagnetic laboratories for the past 20 years. Developed in the last decade, researchers are now using SQUID microscopes (SMs) that are able to scan high resolution maps of a sample's magnetic field. Using this technology, it is possible to display microscale distributions of magnetism within a sample. Furthermore, SM can have sensitivity up to $10^{-15}\mathrm{Am}^2$ while moment magnetometers are only sensitive up to $10^{-12}\mathrm{Am}^2$.

While SQUID moment magnetometers are still better suited for measuring larger, bulk samples with homogeneous magnetization distributions, SMs have clear advantages when studying thin sections of geological samples containing small or complex magnetic sources. If a sample has multiple minerals or multiple magnetic orientations, regions can be constrained and analyzed individually using SM's—a feat that is not possible using a standard moment magnetometer.

Scanning at a constant height above a sample, SQUID microscopes map a planar grid of measurements of the vertical component of the magnetic field generated by the specimen under analysis. In order to raster high resolution scans (50-100 μm), samples need to be close (80-200 μm) to the sensor. Along with this, the sensor needs to be cooled to 4.2 K by liquid helium. Until recently, samples needed to be cooled down to 77 K in order to scan high resolution maps. SM's that scanned samples at room temperature were available, but resolution for these microscopes was on the order of mm, too low for most paleomagnetic research. Cooling samples to 77K is not an option in paleomagnetic research because low temperatures agitate phase changes or magnetic transitions in many common minerals. For example hematite's morin transition occurs around 260K, and magnetite's Verwey transition occurs around 125K (Weiss, Lima, Fong, & Baudenbacher, 2007). Furthermore, many minerals that are superparamagnetic at room temperature can become single domain at lower temperatures. Recently developed (Baudenbaucher 2002) high-resolution SQUID microscopes have the ability to scan samples at room temperature, broadening the application of SM's to include paleomagnetic research.

In order to understand the orientation and strength of the dipole moment, raw magnetic field scans from SM can be modeled as a grid of dipoles (also referred to as a dipole distribution or source distribution in this paper). The mathematics required to make these conversions (explained in the Theory section of this paper) requires a matrix inversion that optimizes the best values for the magnitude and orientation of dipoles. Unfortunately, these optimizations are not perfect. They can amplify noise and yield misleading results. In addition to this, the limitations imposed by Maxwell's equations, noise inherent in all measurements, and data lost in computational approximations further complicate this ill-posed problem. A magnetic scan can often be produced by multiple source distributions. In order to mine the data for the most promising solutions, a proper balance of constraints and regularization must be applied. This thesis explores ways to apply these constraints and regularization techniques by assessing their effectiveness on a simulated magnetic scan with a known source distribution. The most effective of these techniques are applied to a real magnetic scan of shocked basalt and a scan of a small piece of refrigerator magnet.

2. Measurement method for SQUID microscope

SM microscopes typically scan the magnetization of thin section samples using horizontal grid spacing 50-100 μm at a sample-to-sensor distance of 80-200 μm. Although scans of samples with rough surfaces require a higher sample-to-sensor distance in order to account for the uneven height. To keep distances as small and precise as possible, a spring loaded mechanism presses the sample against the sapphire window that insulates the room temperature sample from the 4.2K SQUID sensor. A sheet of 15 μm mylar is often placed over the sample to reduce friction and prevent scratching during measurement.

Figure 1. SQUID Microscope Measurement Configuration

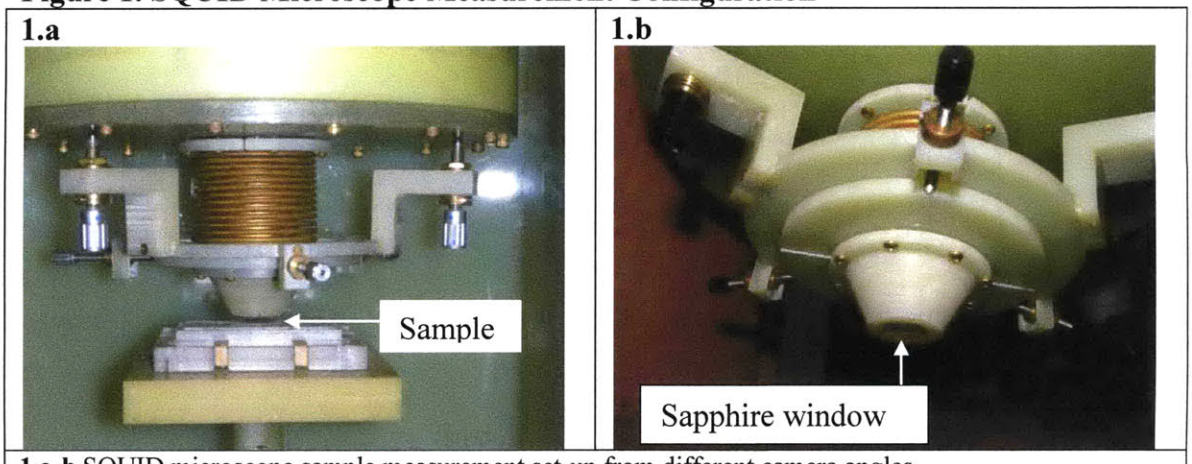

1.a-b SQUID microscope sample measurement set-up from different camera angles

3. Retrieving Dipole distributions from Magnetic Maps

Least Squares Method:

Most SQUID microscopes (an exception, for example, being Ketchen et al., 1997) measure only the vertical component B_z of the magnetic field of a sample. From this vertical component B_z it is possible to retrieve the two horizontal components B_x and B_y using an algorithm in the Fourier domain (Lima & Weiss, 2009). For the sake of simplicity, this section will describe how to estimate a magnetic dipole distribution using only the vertical component B_z of the magnetic scan (Weiss, Lima, Fong, & Baudenbacher, 2007). The results are easy to extend to inversions of all three components of the field.

Figure 2. Magnetic Measurements with Dipole

Magnetic field measurements at a set distance above a sample are used to construct a dipole field

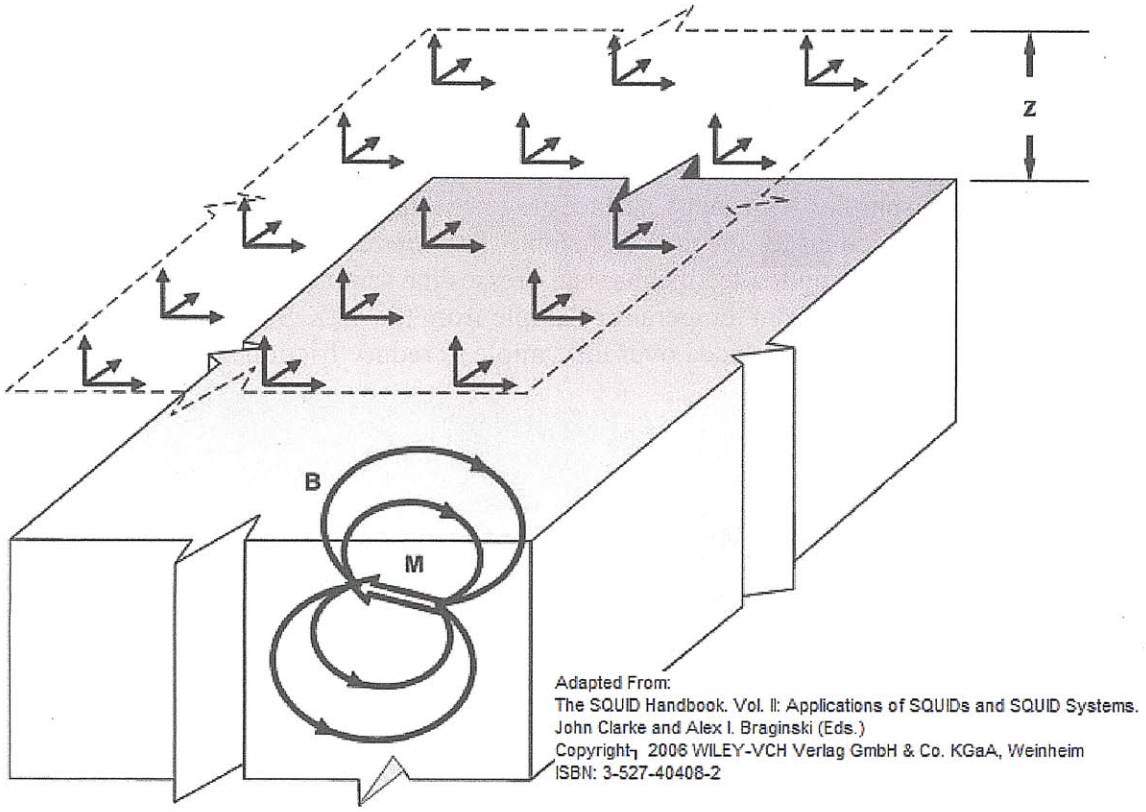

The magnetic field measurement of B_z at position $\vec{a} = (x_a, y_a, z_a)$ near a sample with volume V can be described as

$$B_z(\vec{a}) = \int_V \vec{G}_z(\vec{a}, \vec{b}) \cdot \vec{M}(\vec{b}) dV , \qquad (1)$$

where $\vec{M}(\vec{b})$ is the magnetization at location $\vec{b} = (x_b, y_b, z_b)$ within the sample and $\vec{G}_z(\vec{a}, \vec{b})$ is the Green's function which describes dependence of B_z at the location $\vec{a}$ to the magnetic element at location $\vec{b}$.

Green's function (Weiss, Lima, Fong, & Baudenbacher, 2007) can be described as

$$\vec{G}_z(\vec{a},\vec{b}) = \frac{\mu_0}{4\pi}\frac{3\vec{r}(z_a - z_b) - r^2\hat{k}}{r^5}, \tag{2}$$

where $\hat{k}$ is a vertical unit vector oriented along the z axis, $\vec{r} = \vec{a} - \vec{b}$, and μ_0 is the permeability of free space. In our case, the sample is assumed to be an infinitely thin plane with an area of A oriented normal to the unit vector $\hat{k}$. If we define $x = x_a - x_b$, $y = y_a - y_b$, $z = z_a - z_b$, it is possible to expand equation (1.) into

$$\mathrm{B_z}(\vec{a}) = \frac{\mu_0}{4\pi}\int_A \left[\frac{3zx}{r^5}M_x(x_b,y_b,z_b) + \frac{3zy}{r^5}M_y(x_b,y_b,z_b) + \left(\frac{3z^2}{r^5} - \frac{1}{r^3}\right)M_z(x_b,y_b,z_b)\right]dA. \tag{3}$$

In the equation above (Weiss, Lima, Fong, & Baudenbacher, 2007), the magnetization or moment density (moment per unit area) of the sample is dissected into three components, M_x, M_y, M_z. A common way of discretizing equations 1 and 3 consists of replacing the continuous magnetization distribution $\vec{M}$ with an evenly spaced distribution of Q individual dipoles with moments $\vec{m}_j$. If the spacing between adjacent dipoles is sufficiently fine (as dictated by the distance between the sources and the sample), such an approximation is often adequate to represent the physical sources of magnetic field present in a geological sample. Hence, we can model the measurements of the z-component of the magnetic field B_{zi} made at P locations as

$$\mathrm{B_{zi}} = \sum_{\mathrm{j}=1}^{\mathrm{Q}} \vec{\mathrm{G}}_{\mathrm{zij}}(\vec{\mathrm{a}},\vec{\mathrm{b}}) \cdot \vec{\mathrm{m}}_{\mathrm{j}}(\vec{\mathrm{b}}), \tag{4}$$

where $i = 1,2,\ldots,P$.

Equation 4 can be expanded into

$$\mathrm{B_{zi}} = \frac{\mu_0}{4\pi}\sum_{\mathrm{j}=1}^{\mathrm{Q}} \frac{3z_{ij}x_{ij}}{r_{ij}^5}m_{xj} + \frac{3z_{ij}y_{ij}}{r_{ij}^5}m_{yj} + \left(\frac{3z_{ij}^2}{r_{ij}^5} - \frac{1}{r_{ij}^3}\right)m_{zj}, \tag{5}$$

where $x_{ij} = x_{ai} - x_{bj}$, $y_{ij} = y_{ai} - y_{bj}$, $z_{ij} = z_{ai} - z_{bj}$, $r_{ij} = \sqrt{x_{ij}^2 + y_{ij}^2 + z_{ij}^2}$. The components of $\vec{m}_j$ are m_{xj}, m_{yj}, m_{zj}. By describing the dipole moments in terms of their orientation (i.e., in spherical coordinates) $m_{xj} = m_j \sin\theta_j cos\varphi_j$, $m_{yj} = m_j \sin\theta_j \sin\varphi_j$, $m_{zj} = m_j cos\theta_j$ we can rewrite equation (5.) as.

$$B_{zi} = \frac{\mu_0}{4\pi}\sum_{j=1}^{Q}\left[\frac{3z_{ij}\,x_{ij}}{r_{ij}^5}m_j \sin\theta_j cos\varphi_j + \frac{3z_{ij}\,y_{ij}}{r_{ij}^5}m_j \sin\theta_j \sin\varphi_j + \left(\frac{3z_{ij}^2}{r_{ij}^5} - \frac{1}{r_{ij}^3}\right)m_j cos\theta_j\right]. \quad (6)$$

Previous studies (Weiss, Lima, Fong, & Baudenbacher, 2007) have estimated moments employing various *least squares methods*. In least squares methods, we minimize the squared Euclidean norm D^2 of the difference of the measured field values and the field generated by our approximated solution at the same locations.

$$D^2 = \sum_{j=1}^{Q}\left[\hat{B}_{zi} - \vec{G}_{zij}(\vec{a},\vec{b})\cdot\vec{m}_j^*(\vec{b})\right]^2. \quad (7)$$

In the equation above, $\hat{B}_{zi}$ is the symmetrical rectangular grid of measured vertical components of the magnetic field and $\vec{m}_j^*$ are the estimated dipole moments of the dipole distribution. Because each of the Q dipoles is decomposed into three components, without further constraints there are $3Q = N$ parameters to solve for.

Equation 4 shows that the magnetic field is linearly related to the dipole moments. Therefore, we can express the system of linear equations in matrix form $\boldsymbol{Ad} = \hat{\boldsymbol{b}}$, where $\boldsymbol{A}$ is the $M \times N$ Jacobian (Green's matrix) (Weiss, Lima, Fong, & Baudenbacher, 2007),

$$\boldsymbol{A} = \begin{bmatrix} \partial B_{z1}/\partial m_{x1} & \partial B_{z1}/\partial m_{y1} & \partial B_{z1}/\partial m_{z1} & \partial B_{z1}/\partial m_{x2} & \partial B_{z1}/\partial m_{y2} & \partial B_{z1}/\partial m_{z2} & \cdots & \partial B_{z1}/\partial m_{zQ} \\ \partial B_{z2}/\partial m_{x1} & & & & & & & \\ \vdots & & & & & & & \vdots \\ \partial B_{zP}/\partial m_{x1} & & & & & & & \partial B_{zP}/\partial m_{zQ} \end{bmatrix}.$$

And from Eq. (5.)

$$\begin{aligned} \partial B_{zi}/\partial m_{xi} &= \mu_0 3z_{ij}\,x_{ij}/4\pi r_{ij}^5 \\ \partial B_{zi}/\partial m_{yi} &= \mu_0 3z_{ij}\,y_{ij}/4\pi r_{ij}^5 \\ \partial B_{zi}/\partial m_{zi} &= \mu_0 3z_{ij}^2/4\pi r_{ij}^5 - \mu_0/4\pi r_{ij}^3, \end{aligned} \quad (8)$$

where $\boldsymbol{d}$ is an $N \times 1$ vector containing the values of the dipole moments reduced to their component values,

$$\boldsymbol{d} = \left[m_{x1}\ m_{y1}\ m_{z1}\ m_{x2}\ m_{y2}\ m_{z2} \cdots m_{zQ}\right]^T,$$

and $\hat{\boldsymbol{b}}$ is an $M \times 1$ vector containing magnetic field measurements.

$$\hat{\boldsymbol{b}} = \left[\hat{B}_{z1}\ \hat{B}_{z2} \cdots \hat{B}_{zP}\right]^T.$$

The model dipole distribution $\boldsymbol{d}$ is approximated by determining $\boldsymbol{d}^*$ through least squares approach. To do this, the residual norm $\|\boldsymbol{A}\boldsymbol{d}^* - \widehat{\boldsymbol{b}}\|$ is minimized using the Euclidian norm between the measured data and the field generated by the modeled dipole distribution. Simply put, residuals represent the mismatch between the modeled and measured map. This mismatch is caused by the limited information reserved in the finite resolution of the field maps, as well as noise and uncertainties inevitably present in experimental data.

When approximating the source distribution it is important to understand the limitations of the model. In general, the magnetic inverse problem is severely non-unique (Clarke & Braginski, 2006). Discretization of the source model and field maps further aggravates this issue. Without further constraints, there may be multiple or even infinite dipole distribution solutions that explain the experimental data. However, these multiple solutions may be distinguished because some are more realistic representations of the physical sources of magnetic field present in the sample than others. Although a smaller residual norm usually indicates a better solution, the solution with the smallest residual norm is not necessarily the best physical solution. In order to extract meaningful solutions from the data, we need to apply a balance of constraints and regularization techniques as well as a variety of metrics to compare their abilities to determine an accurate source distribution.

4. Constraints

Unidirectional Solution:

A variety of geological samples like freshly cooled lavas and unaltered sedimentary rocks exhibit unidirectional behavior, owing to the physical and chemical processes that rocks may experience upon formation or subsequent alteration. In this study, we focused on unidirectional magnetization distributions, as they allow us to investigate relevant terrestrial and extraterrestrial samples while improving uniqueness and retaining mathematical tractability. Thus, the elements of the modeled dipole distributions have identical orientation (θ, φ) and varying magnitude (Weiss, Lima, Fong, & Baudenbacher, 2007). We will explore modeled fields by applying two modes, bipolar and unipolar. Bipolar dipole distribution models will be free to have negative and positive values, whereas unipolar field models will be constrained to purely non-negative dipole distribution values ($m_j \geq 0$ for all j). By constraining the orientation of the dipole distribution, we can redefine the matrices

$$\boldsymbol{d} = \begin{bmatrix} m_1 & m_2 \cdots m_Q \end{bmatrix}^T$$

$$A = \begin{bmatrix} \partial B_{z1}/\partial m_1 & dB_{z1}/dm_2 & \cdots & \partial B_{z1}/\partial m_Q \\ \partial B_{z2}/\partial m_1 & & & \\ \vdots & & & \vdots \\ \partial B_{zP}/\partial m_1 & & \cdots & \partial B_{zP}/\partial m_Q \end{bmatrix},$$

where

$$\frac{\partial B_{zi}}{\partial m_j} = \frac{\mu_0}{4\pi}\frac{3z_{ij}x_{ij}}{r_{ij}^5}\sin\theta\cos\varphi + \frac{\mu_0}{4\pi}\frac{3z_{ij}y}{r_{ij}^5}\sin\theta\sin\varphi + \frac{\mu_0}{4\pi}\left(\frac{3z_{ij}^2}{r_{ij}^5} - \frac{1}{r_{ij}^3}\right)\cos\theta. \quad (9)$$

And for all j

$$m_{zj} = \frac{\cot\theta}{\cos\varphi}m_{xj} \text{ and } m_{yj} = m_{xj}\tan\varphi. \quad (10)$$

With the orientation of the dipoles constrained, we can describe the three components of a magnetic moment knowing only one. This provides a model where $N = Q$ parameters instead of the unconstrained model where $N = 3Q$ parameters.

5. Regularization

Tikhonov Regularization

Often minimizing the residual norm $\|\boldsymbol{A}\boldsymbol{d}^* - \widehat{\boldsymbol{b}}\|$ alone is not sufficient to arrive at an acceptable solution and more sophisticated regularization techniques are applied to derive better results from the data. This study explores ways to find solutions through Tikhonov regularization (Hansen, 1994). Tikhonov regularization searches for a solution by minimizing

$$\boldsymbol{x}_\lambda = \|\boldsymbol{A}\boldsymbol{d}^* - \widehat{\boldsymbol{b}}\|_2^2 + \boldsymbol{\lambda}^2\|\boldsymbol{L}\boldsymbol{d}^*\|_2^2, \quad (11)$$

which is a combination of the residual norm (first term) and a weighted side constraint (second term). In the equation above, the stabilizing operator $\boldsymbol{L}$ is used to specify the side constraint. The matrix $\boldsymbol{L}$ can be constructed to fit the context of the problem. Its core function is to reduce noisy components or nonrealistic solutions. In this study, $\boldsymbol{L}$ is either the unity matrix—in which case the norm of the solution is minimized—or a matrix representing a high-pass filter that reduces high frequency oscillations between positive and negative moment values over the spatial distribution. To distinguish between the two methods, we refer *high-pass Tikhonov regularization* when $\boldsymbol{L}$ is conditioned to be a high-pass filter and we refer to *Tikhonov regularization* when $\boldsymbol{L}$ is set to the identity matrix. The regularization parameter $\boldsymbol{\lambda}$ controls the weight of the side constraint. Setting $\boldsymbol{\lambda} = \boldsymbol{0}$ is equivalent to applying the unregularized least squares method, whereas making $\boldsymbol{\lambda}$ large leads to solutions dominated by the side constraint.

Regularization improves the quality of the solution because smaller-norm source distributions (or distributions where high-frequency components are small) are less likely to have high spatial frequency magnetization patterns. As $\boldsymbol{\lambda}$ increases, the magnitude of the source distribution (or of the high-frequency components) will decrease while the residuals will increase, such that, a $\boldsymbol{\lambda}$ that is too high can produce a source distribution that is too weak or too smooth. There is often a choice of lambda which optimizes the tradeoff between over smoothing the solution and over fitting the data with low residuals.

Singular Value Decomposition

Another regularization tool applied in this study is truncated singular value decomposition (TSVD). Since $A \in \mathbb{R}^{M \times N}$ and is a rectangular matrix with $M \geq N$, the singular value decomposition (SVD) of A will be

$$\boldsymbol{A = U\Sigma V^T = \sum_{i=1}^{N} u_i \sigma_i v_i^T,} \tag{12}$$

where $\boldsymbol{u_i}$ and $\boldsymbol{v_i}$ are the left and right singular vectors of $\boldsymbol{A}$, $\boldsymbol{U = (u_1, \ldots, u_N)}$, and $\boldsymbol{V = (v_1, \ldots, v_N)}$. The matrices $\boldsymbol{U}$ and $\boldsymbol{V}$ have orthonormal columns: $\boldsymbol{U^T U = V^T V = I_N}$. $\boldsymbol{\Sigma}$ is a diagonal matrix with the singular values of $\boldsymbol{A}$ $\boldsymbol{(\sigma_1, \ldots, \sigma_N)}$ arranged in non-increasing order $\boldsymbol{(\sigma_1 \geq \cdots \geq \sigma_N \geq 0)}$. As $\boldsymbol{i}$ increases, the singular values of $\boldsymbol{\sigma_i}$ gradually decay to zero.

After decomposing the matrix $\boldsymbol{A}$ with SVD, we determine $\boldsymbol{A^{-1}}$ and find $\boldsymbol{d}$ by $\boldsymbol{A^{-1}\hat{b} = d^*}$. It is possible to find the $\boldsymbol{A^{-1}}$ using the property

$$\boldsymbol{A^{-1} = V\Sigma^{-1}U^T.} \tag{13}$$

In what this paper refers to as *soft TSVD* we define $\boldsymbol{\Sigma^{-1}}$ as a diagonal matrix of values

$$\boldsymbol{\Sigma^{-1} = \sum_{i=1}^{N} \frac{1}{\sigma_i} \cdot \frac{\sigma_i}{\gamma + \sigma_i},} \tag{14}$$

where $\boldsymbol{\gamma}$ is a varied parameter that can be manipulated to control the magnitude of $\boldsymbol{\Sigma^{-1}}$ and prevent small values $\boldsymbol{\sigma_i}$ from approaching infinity during the inversion process. This regularization method is referred to as "soft' because it tapers off the smaller values of $\boldsymbol{\sigma_i}$ smoothly as opposed to *hard TSVD*, which defines $\boldsymbol{\Sigma^{-1}}$ as

$$\boldsymbol{\Sigma^{-1} = \sum_{i=1}^{\gamma} \frac{1}{\sigma_i},} \tag{15}$$

where $\boldsymbol{\gamma}$ is a number smaller than $\boldsymbol{N}$ used to remove the smaller, less significant values of $\boldsymbol{\sigma_i}$ from the data. Tapering (soft TSVD) or removing (hard TSVD) small values of $\boldsymbol{\sigma_i}$ reduces detrimental influences of noisy measurements and errors in computational approximations that are amplified during the inversion process.

6. Application

Simulation:

We tested the effectiveness of the constraints and regularization techniques on a synthetic magnetic map with a known magnetic field. The map we tested was made up of extended strips of continuous, uniform magnetization shaped as the 'M' of the MIT logo. The magnetization intensity of the 'M' and the orientation (θ,φ) could be manipulated in a controlled manner. To better simulate real measurements, we applied white noise and position noise.

$$\text{White Noise} = \Psi_W\left[\text{randn}(\max(\widehat{B}_z) - \min(\widehat{B}_z))\right] \qquad (16)$$

White noise simulates the Gaussian distributed noise common during actual magnetic microscopy measurements. It is controlled by percent Ψ_w of the peak-to-peak value (computed over the whole map) of the magnetic field. In studies testing white noise, every measurement has white noise added to the ideal magnetic field value. Unless otherwise specified, we assume $\Psi_w = .05$ in this paper (125 decibel signal-to-noise ratio). This amount of noise simulates an extreme case where the levels of noise are larger than what is found in most magnetic microscopy measurements.

Position noise simulates the measurement error inherent in the (x,y) position of the sensor by adding a range of random values to the location of every measurement. In this study, position noise will always add a distance ranging from 0nm to 50 nm unless otherwise specified.

Real Samples

This study applies the most effective modes of regularization on two real samples, a shocked basalt and a refrigerator magnet. The SQUID microscope scan of the shocked basalt comes from a previous study (Gattacceca, Boustie, Lima, Weiss, de Resseguier, & Cuq-Lelandais, 2010), but a more complete analysis of the rock's petrography and magnetic properties can be found in (Gattacceca, Berthe, Boustie, Vadeboin, Rochette, & de Resseguier, 2008). The thin section of the shocked basalt has dimensions 10 mm tall, 9.5 mm in diameter and 0.5 mm thick. In a previous study, the sample was demagnetized with an alternating field (AF) and then given an initial thermal remnant magnetization (TRM) in an ambient field of intensity between 50 and 300 μT. The magnetization of the shocked basalt was then scanned by the SQUID microscope in MIT Paleomagnetism Laboratory (www.mit.edu/paleomag) with 121 × 121 (150 μm step size) spatial resolution. The refrigerator magnet measures 20 mm × 140 mm and uses data from a 36 × 48 (5 mm step size) magnetometer measurement.

Figure 3. Photographs of Shocked Basalt and Refrigerator Magnet

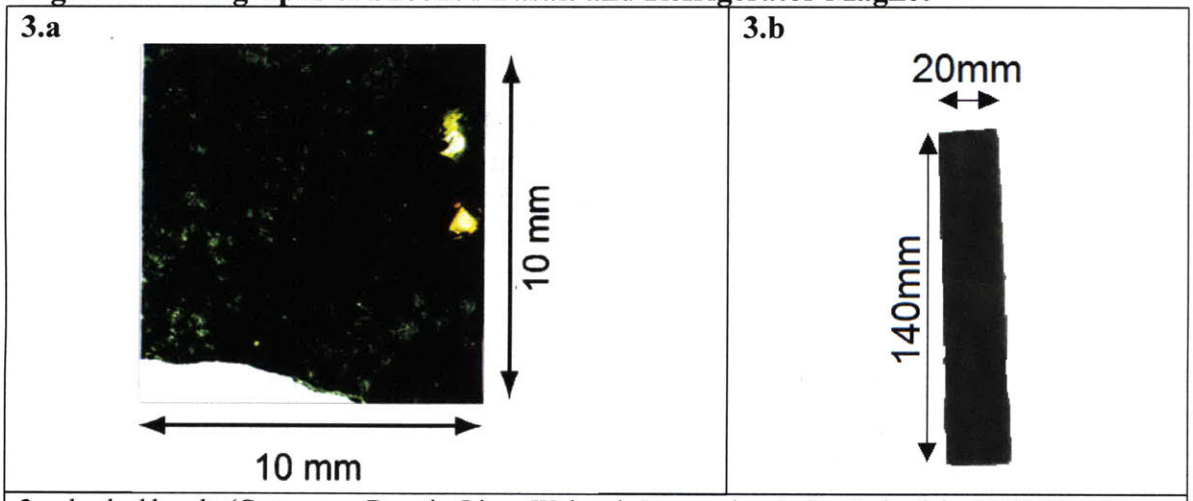

3.a shocked basalt (Gattacceca, Boustie, Lima, Weiss, de Resseguier, & Cuq-Lelandais, 2010) **3.b** refrigerator magnet

Analysis Methods

With simulated data, where the ideal source distribution $\boldsymbol{d}$ is known, it is possible to compare it to the recovered source distribution, $\boldsymbol{d}^*$. This is a powerful tool in developing effective analysis techniques, but it is limited in application to purely synthetic data, since $\boldsymbol{d}$ is unknown in real samples. Along with qualitatively comparing maps through visual analysis of $\boldsymbol{d}^*$, $\boldsymbol{d}$, and $\boldsymbol{d}^* - \boldsymbol{d}$, we employ the normalized root-mean square deviation (NRMSD) to measure discrepancies, as utilized in a previous study (Lima & Weiss, 2009)

$$NRMSD = \left[\frac{\sum_{j=1}^{Q}\left[\boldsymbol{d}_j^* - \boldsymbol{d}_j\right]^2}{\sum_{j=1}^{Q}\boldsymbol{d}_j^2}\right]^{1/2}. \tag{17}$$

Along with the NRMSD value derived above, to compare $\boldsymbol{d}^*$ to $\boldsymbol{d}$ we map the difference between the source distribution derived by inversion and the ideal source ($\boldsymbol{d}^* - \boldsymbol{d}$). This paper will refer to these maps difference maps.

Although this method is the most direct and therefore the most effective tool for determining the accuracy of the constraints and normalization, we developed other analysis methods that could be applied to both synthetic and real data sets. We can compare the dipole distribution maps indirectly through $\widehat{\boldsymbol{b}}$ and $\boldsymbol{A}\boldsymbol{d}^*$, the measured and computationally generated SQUID scan maps, respectively. We examined $\widehat{\boldsymbol{b}}$ and $\boldsymbol{A}\boldsymbol{d}^*$ and $\boldsymbol{A}\boldsymbol{d}^* - \widehat{\boldsymbol{b}}$ in a similar way we examined the dipole distributions. We also applied normalized root-mean square deviation in order to quantify the differences.

$$\text{normalized residuals} = \left[\frac{\sum_{j=1}^{Q}\left[\boldsymbol{A}\boldsymbol{d}_j^* - \widehat{\boldsymbol{b}}_j\right]^2}{\sum_{j=1}^{Q}\widehat{\boldsymbol{b}}_j^2}\right]^{1/2}. \tag{18}$$

In this study, we refer to the normalized root-mean square deviation of the magnetic field scans as *normalized residuals*. For further analysis we also map the differences between the inversion generated field and the original scan ($\boldsymbol{A}\boldsymbol{d}^* - \widehat{\boldsymbol{b}}$). This paper will refer to these maps as *residual maps*.

While magnetic field comparison can indicate the accuracy of a certain method for recovering a dipole distribution, it is important to understand the limits of this analysis. There can be many or possibly infinite dipole distribution solutions for any magnetic field scan. And although it is fair to say that solutions with lower normalized residuals tend to better represent the actual dipole distributions, a solution with the lowest normalized residuals is not necessarily the most accurate dipole distribution.
A common problem that occurs when modeling bipolar solutions with low normalized residuals is that dipoles tend to oscillate between positive and negative magnitude with unrealistic frequency. While such oscillations may produce a solution that is theoretically a better mathematical fit for the model, these source distributions are poor indicators of any real phenomenon. It is possible to tame this problem by constraining the dipoles in unipolar analysis, but it is also at times advantageous to merely limit (instead of completely eliminating) unreal negative dipoles. In controlled situations where the magnitude of the dipoles must be positive, such as synthetically generated

fields and samples with strongly defined orientation (shocked basalt), we can sum the square of negative dipole values and compare that to the known total magnetic moment of the object as a test of the accuracy of the inversion. These values can be evaluated alone in isolated form or multiplied by normalized residuals values to create a mixed parameter analysis that can determined a balanced minimum of normalized residuals and the negative values of the dipole distribution. When examining data it is important to note that unipolar inversions have no negative values in their source distribution. Therefore, summed negative values and mixed parameter analysis do not apply to unipolar analysis.

7. Results and Analysis

Synthetic Scans

In order to apply the methods discussed above to magnetic microscopy maps, we must evaluate their effectiveness on synthetic data. We used as synthetic sources three magnetic strips arranged in the shape of the letter "M" of the MIT logo (Figure 4.a). The strips were homogeneously magnetized in a specific direction and were used to generate synthetic magnetic field maps such as the one shown in Figure 4.b. Because these synthetic source distributions are continuous and the analytical expression for their magnetic field is known, they constitute a useful tool for analyzing the quality of the inverse solution as well as the effects of source discretization. In order to create an ideal discretized source distribution to test the inversions (Figure 4.c), we divided up the distribution in small square elements of constant magnetization. The magnetization strength of each element was calculated according to the fraction of a slab that fell within the area of the element, so as to correctly account for the edges of the slabs. We then modeled each element as a magnetic dipole and multiplied the ideal source distribution by the calculated Green's matrix ($\boldsymbol{Ad}$) to generate the corresponding synthetic field map. To quantify the error due to source discretization, we subtract the field map of the continuous distribution from the map of the discretized distribution (i.e., $\boldsymbol{Ad} - \boldsymbol{b}$), as depicted in Figure 4.d.

Figure 4. Generating the Ideal Source distribution of a Synthetic Map

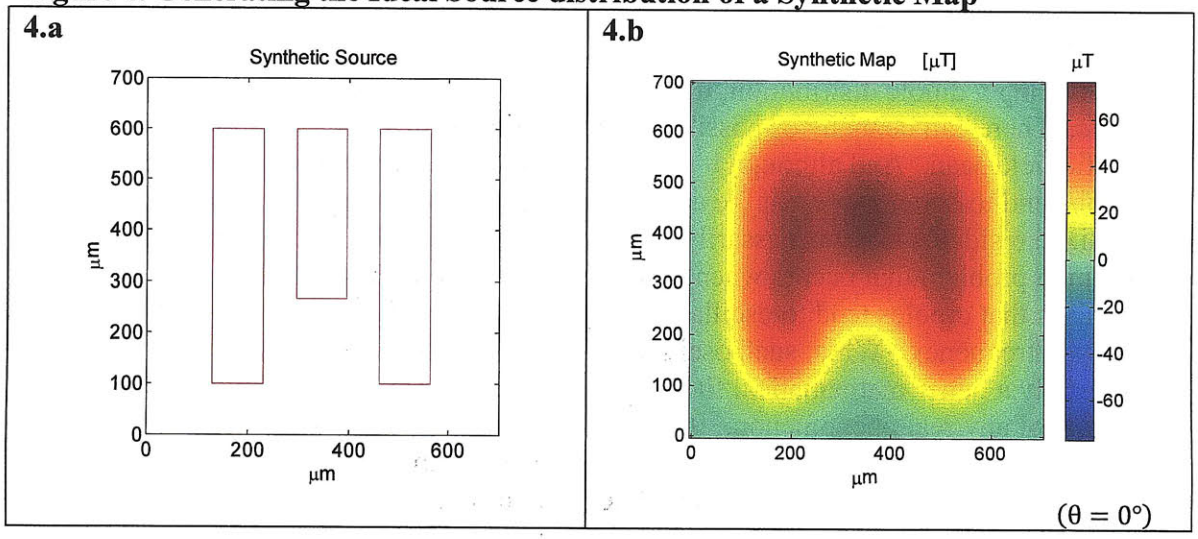

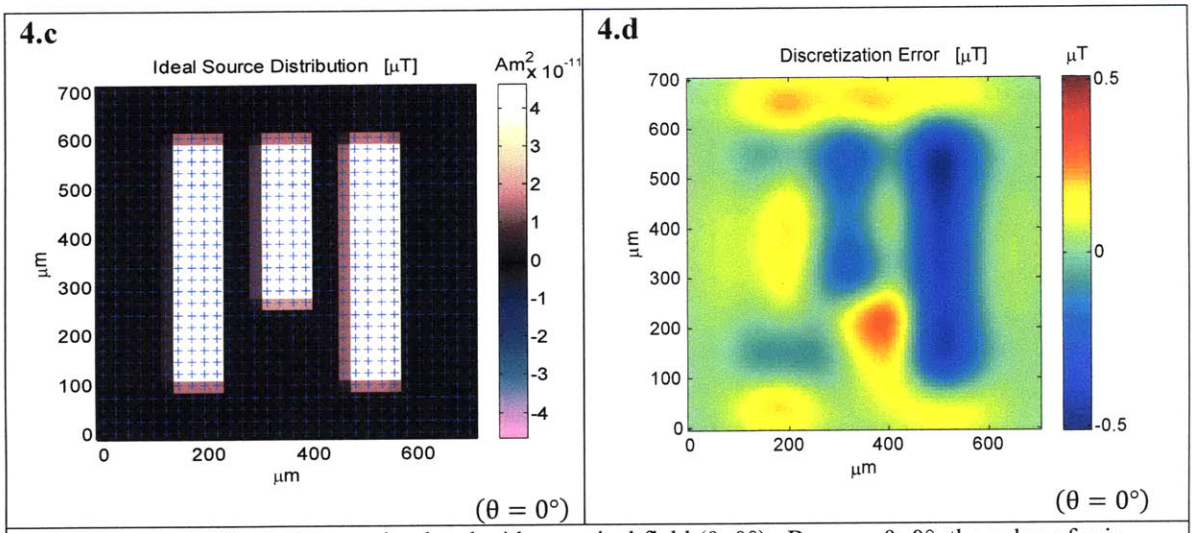

Measurements in Figure 4. were simulated with a vertical field (θ=0°). Because θ=0°, the value of φ is irrelevent. The 700×700 μm sample area is scanned with 90×90 resolution and modeled with a 30×30 dipole distribution. Like all synthetic fields in this study, the sample to sensor distance is 150μm. **4.a** The dimensions of the synthetic sample with uniform magnetic intensity. **4.b** The magnetic field map of the synthetic sample (z-component of the field). **4.c** The discretized distribution of the synthetic sample. **4.d** Difference between the field maps generated by the discretized (4.c) and non-discretized (4.a) source distributions (normalized residuals = 3.73×10^{-3}.)

Although the shapes of the magnetic strips are always the same, we can vary the direction of their magnetization, thereby changing its magnetic field. Evidently, the magnitude of the ideal source distribution remains the same.

Figure 5. Effects of source discretization for (θ=45°, φ=30°) and (θ=90°, φ=30°)

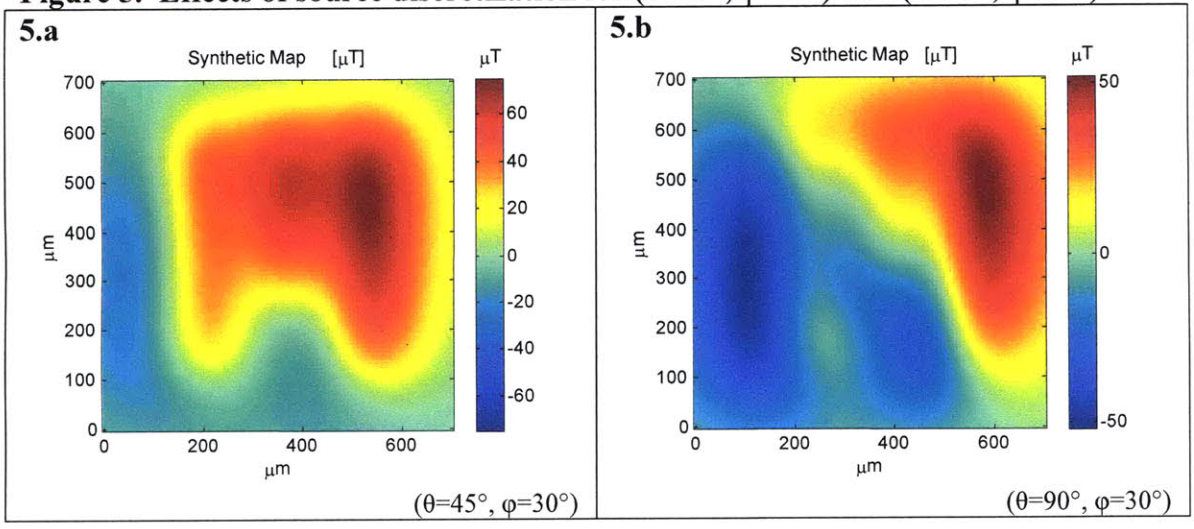

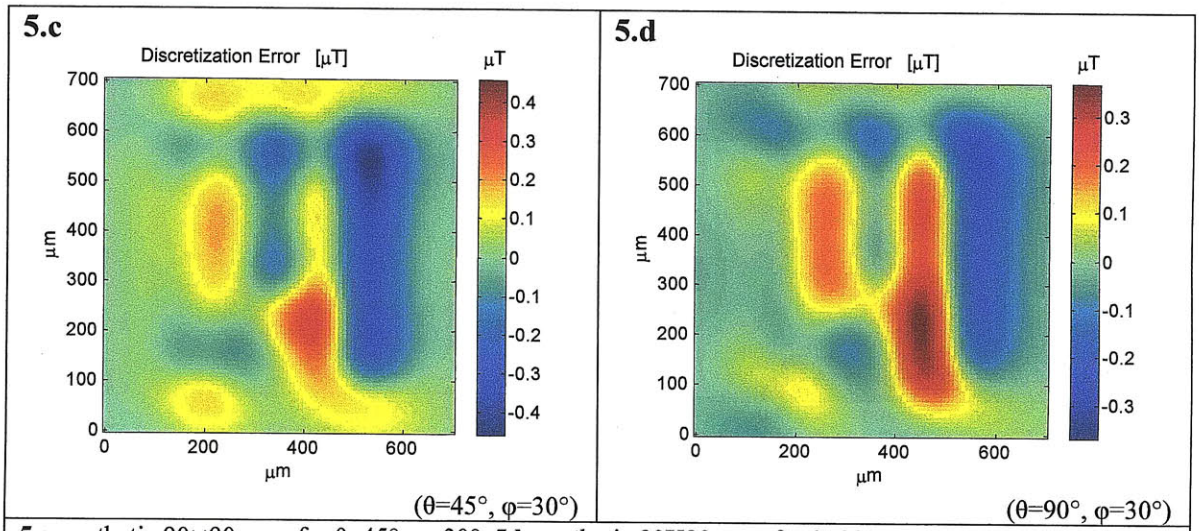

5.a synthetic 90×90 scan for θ=45°, φ=30°. **5.b** synthetic 90X90 scan for θ=90°, φ=30°. **5.c** error resulting from a 30×30 discretization of the synthetic source used in 4.a (normalized residuals= 3.87×10^{-3}). **5.d** error resulting from a 30×30 discretization of the synthetic source used in 5.b (normalized residuals= 4.21×10^{-3}).

In order to assess the pervasive effects of noise on the inversions, we added Gaussian white noise or position noise to synthetic maps when appropriate, as illustrated in Fig. 6.

Figure 6. Maps of Noisy Measurements

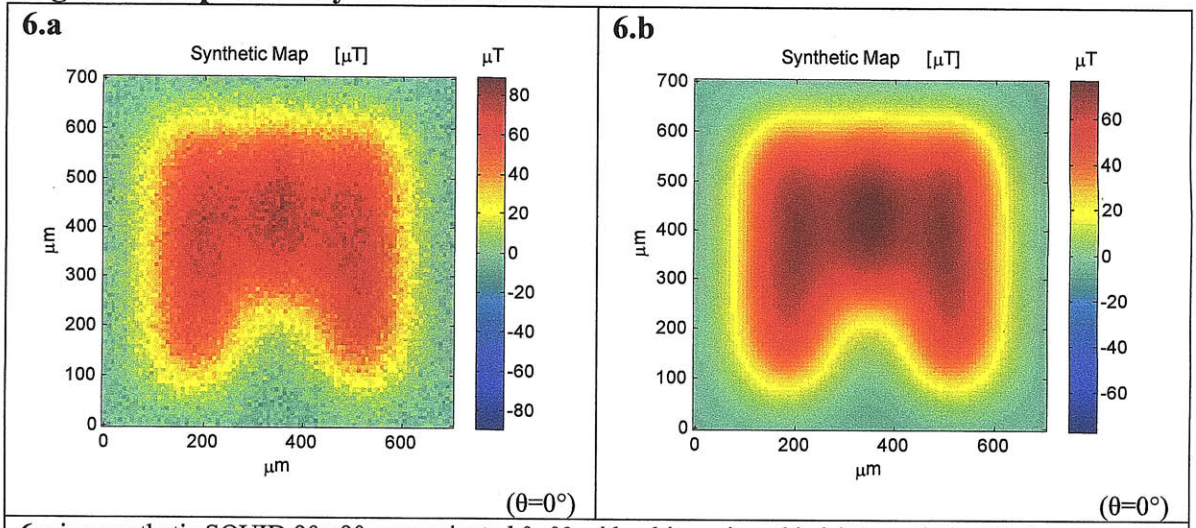

6.a is a synthetic SQUID 90×90 scan oriented θ=0° with white noise added ($\Psi_w = 5\%$). **6.b** is a synthetic SQUID 90×90 scan oriented θ=0° with position noise added ($\Psi_p = 50$ nm).

Least Squares Method

In noiseless simulations, when the height and orientation is known, bipolar least squares inversions can provide a fairly accurate solution (see figure 7.a-f). An exception to this trend occurs when θ = 90° (see figure 7.g-i). At this orientation, the solution

becomes non-unique and has many possible solutions, making it difficult to determine the proper orientation.

Figure 7. Bipolar Least Squares Inversions

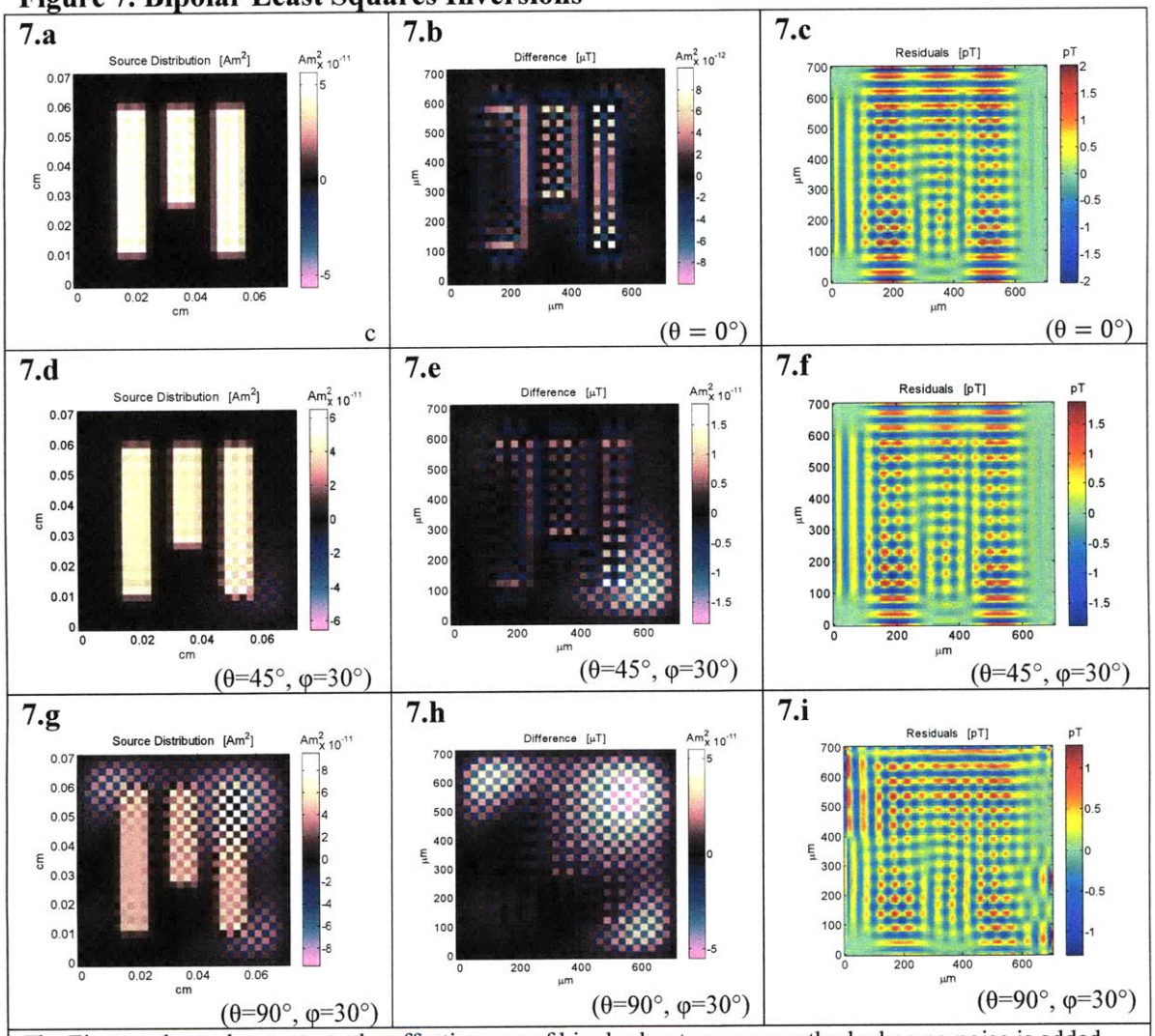

The Figures above demonstrate the effectiveness of bipolar least squares method when no noise is added and the heigh and orientation are known. By analyzing the source distribution, difference between the estimated and ideal solution, and the residuals, it is possible to evaluate the effectiveness of an inversion method. **7.a-c** For θ=0°, NRMSD=0.0914 normalized residuals= 1.5840×10^{-8}, Summed Negative Values=3.2776×10^{-10}, Mixed Parameter Analysis= 5.1916×10^{-18} **7.d-f** For θ=45°, φ=30°, NRMSD=0.1631, normalized residuals=1.5416×10^{-8}, Summed Negative Values= 7.4716×10^{-10}, Mixed Parameter Analysis= 1.1518×10^{-17} **7.g-i** For θ=90°, φ=30°, NRMSD=0.8262, normalized residuals=1.4718×10^{-8}, Summed Negative Values= 4.2821×10^{-9}. Mixed Parameter Analysis= 6.3024×10^{-17}

Often, the orientation of the magnetization distribution within a sample is not known beforehand. In this situation, we can calculate a number of solutions corresponding to different orientations and inspect the normalized residuals or some other measure of the quality of the solution to estimate the correct orientation. Under ideal conditions, the inversion obtained with the correct orientation should have the smallest

error. When no noise is added, bipolar least squares method is effective at estimating proper orientation by means of angle searches (see Figure 8.1). However, when noise is added, least squares method is no longer sufficient (see Figure 6.1). The examples below are bipolar least square inversions of synthetic measurements with white noise added, where the slabs were magnetized in the direction (θ=45°, φ=30°). They are prime examples of failed inversions without regularization, and demonstrate that the smallest errors do not correspond to the correct orientation.

Figure 8.1 θ Search Using Bipolar Least Squares Method with White Noise Added

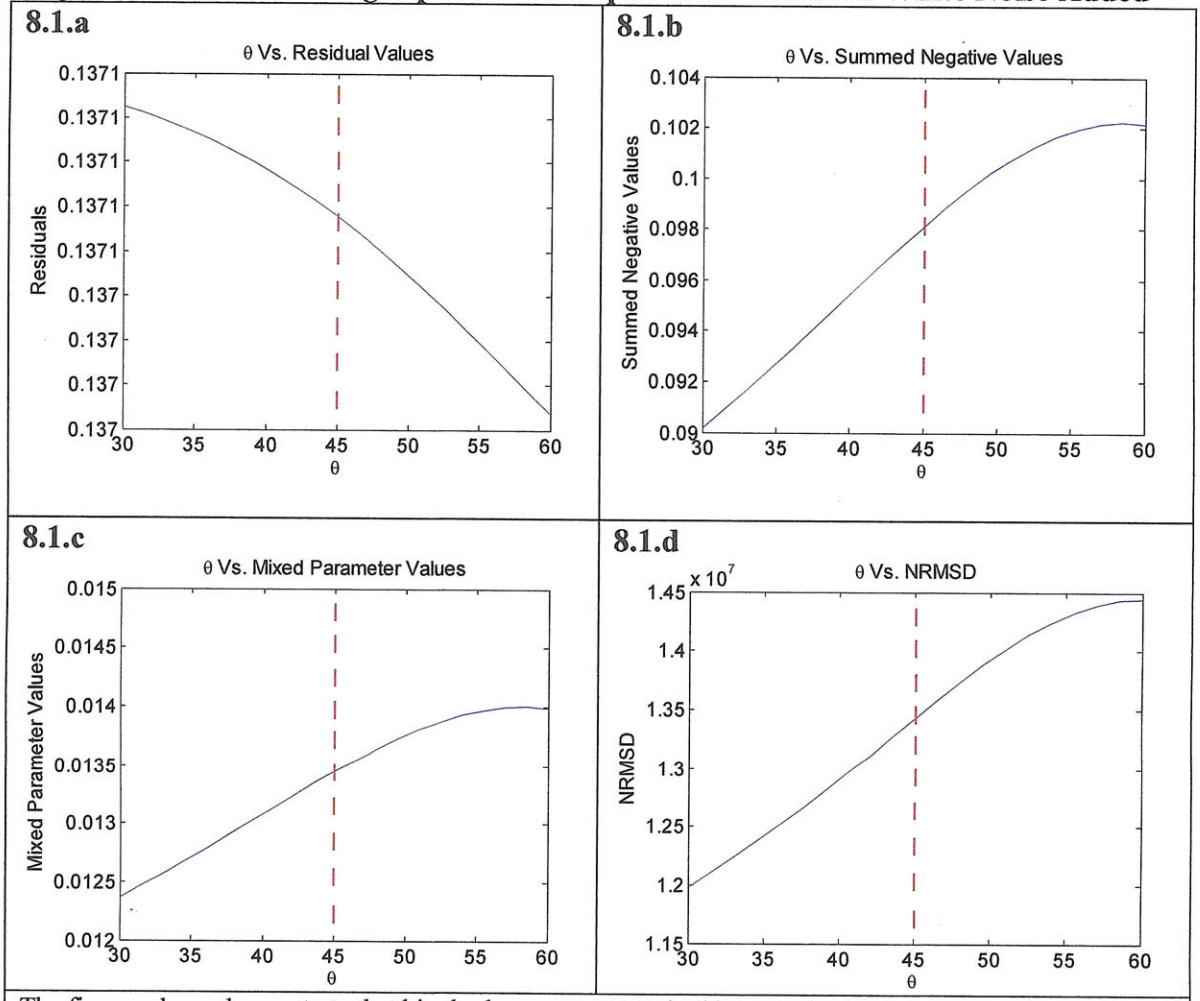

The figures above demonstrate that bipolar least squares method is not effective at searching for the proper orientation when white noise is added. The error indicators should have a minimum at $\theta = 45°$ (marked by the red dotted line) because the correct solution should yield the smallest amount of errors. **8.1.a** is a plot of residual values of bipolar least squares method for a range of angles. **8.1.b** is a plot of summed negative values of bipolar least squares method for a range of angles. **8.1.c** is a plot of mixed parameter values of bipolar least squares method for a range of angles. **8.1.d** is a plot of NRMSD of bipolar least squares method for a range of angles.

Another parameter that is not accurately known beforehand is the sensor-to-sample distance. Even though good estimates can be obtained by scanning a current-carrying wire along a line and fitting a model for the magnetic field, there is usually an uncertainty of ~ ±15 μm in this parameter. Therefore, we can try to improve the accuracy of the

estimate by calculating inversions for different distances and analyzing the error in the solution. Below is another example of a bipolar least squares inversion to estimate model parameters. The nominal height, z, for these simulations is 150 μm. If the inversion methods worked properly, the solution with smallest error should occur at 150 μm. However, height (i.e., sensor-to-sample distance) searches using the bipolar least squares method do not work on samples with noise added, as illustrated in Figure 8.2.

Figure 8.2 Height Search Using Bipolar Least Squares Method with White Noise

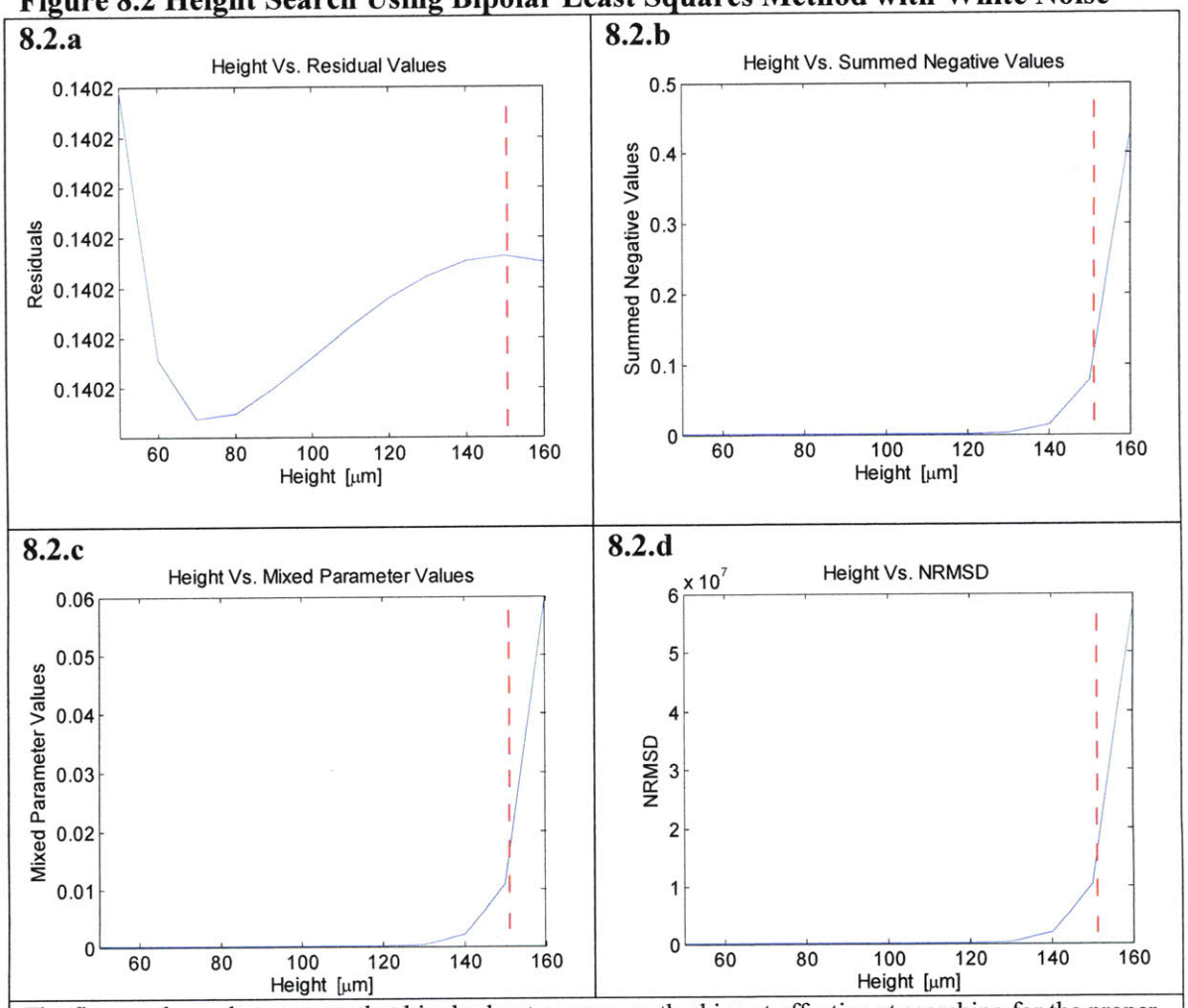

The figures above demonstrate that bipolar least squares method is not effective at searching for the proper height when white noise is added. The error indicators should have a minimum at z = 150 μm (marked by the red dotted line) because the correct solution should yield the smallest amount of errors. **8.2.a** is a plot of residual values of bipolar least squares method for a range of heights. **8.2.b** is a plot of summed negative values of bipolar least squares method for a range of heights. **8.2.c** is a plot of mixed parameter values of bipolar least squares method for a range of heights. **8.2.d** is a plot of NRMSD of bipolar least squares method for a range of heights.

As mentioned before, in addition to NRMSD, we utilized difference maps (i.e., $\boldsymbol{d}^* - \boldsymbol{d}$) to analyze discrepancies in the inverse solutions. We found that with synthetic data with very low noise levels, bipolar inversions are more effective at producing source distributions than unipolar inversions. Bipolar inversions have smaller NRMSD and Residual values, besides being much faster to calculate. Furthermore, they produce maps

that qualitatively appear closer to the ideal source distribution. However, when higher levels of noise are added (both white noise and position noise), bipolar analysis fails at retrieving physical magnetization distributions, and unipolar becomes the more desireable method. Even though unipolar least squares inversions perform better than bipolar least squares inversions for noise field maps, it is important to note that both unregularized least squares methods are still significantly less effective than other regularization techniques.

The source distribution generated from noisy samples through bipolar inversions of least squares method (Figure 8.3) no longer resembles the ideal source distribution. While NRMSDs are seven orders of magnitude larger than in the noiseless case, the residuals in the field map are relatively low, being essentially dominated by additive noise present in the synthetic field map.

Figure 8.3 Bipolar Least Squares Inversions with White Noise

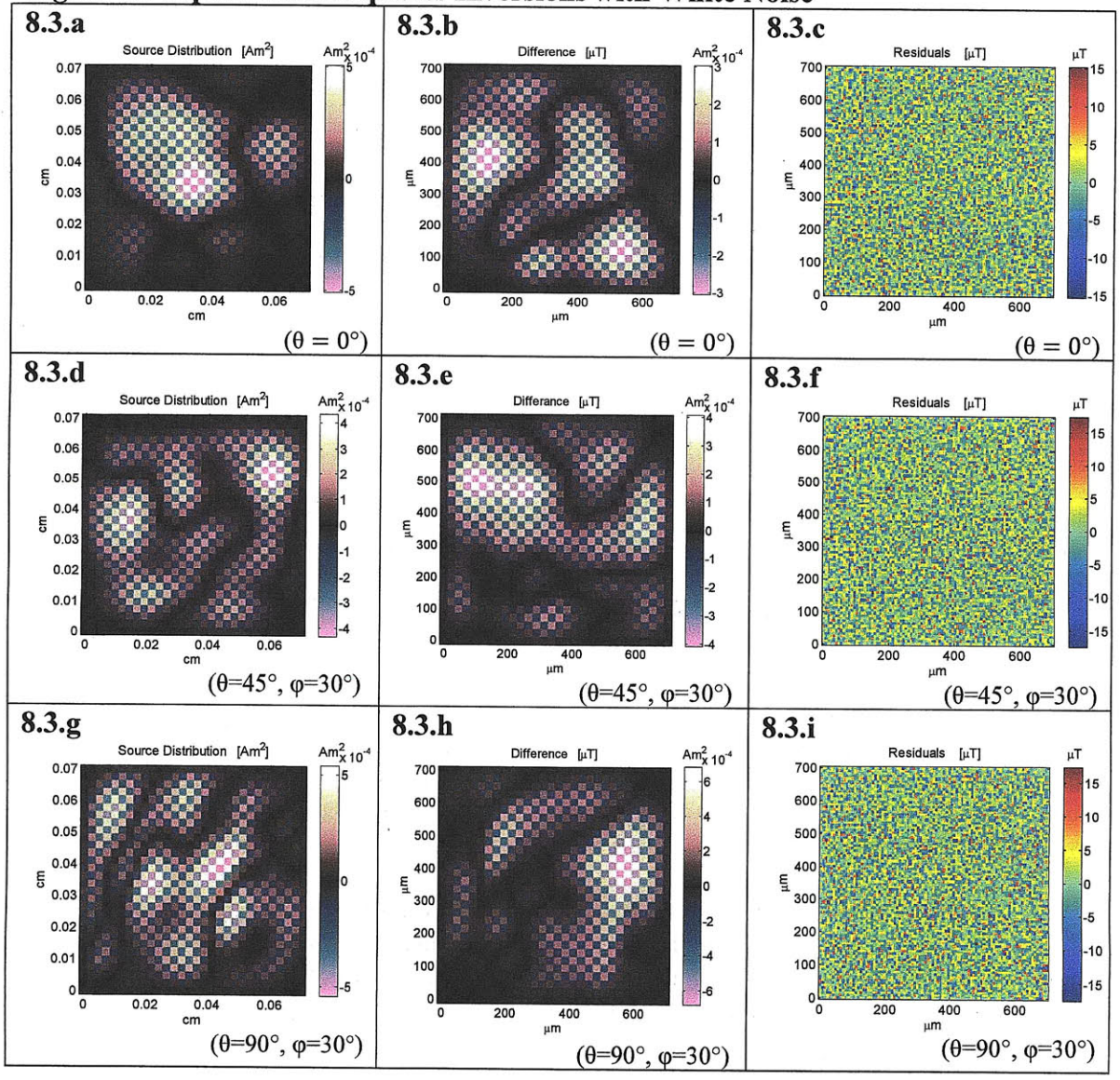

The figures above demonstrate that bipolar least squares method is not effective at finding the solution to measurements with white noise added. The estimated source distributions do not represent the ideal source distributions. **8.3.a-b** NRMSD=4.3355× 10^{6}, Normalized Residuals=1.0256× 10^{-1}, Summed Negative Values= 3.3452× 10^{-2}, Mixed Paramater Values=3.4309× 10^{-3} **8.3.c-d** NRMSD=6.7293e× 10^{6}, Normalized Residuals= 1.3853× 10^{-1}, Summed Negative Values=5.0429× 10^{-2}, Mixed Parameter Analysis=6.9860× 10^{-3} **8.3.e-f** NRMSD=1.4043× 10^{7}, Normalized Residuals=1.7832× 10^{-1}, negcheck=9.4504× 10^{-2}, Mixed Parameter Analysis=1.6852× 10^{-2}

Tikhonov regularization performs significantly better than unregularized least squares method in all metrics of effective evaluations of measurements. The major drawback is that it involves the inversion of matrix with twice the size of the original one. Regular Tikhonov and High-Pass Tikhonov regularization have similar abilities for determining the correct angle of orientation and height, but high-pass Tikhonov yields lower values for Normalized Residuals, Summed Negative Values, Mixed Parameter Analysis, and NRMSD. Even though it increases accuracy of inversions, high-pass Tikhonov takes more computational time to arrive at similar results as conventional Tikhonov. Therefore, it was advantageous in this study to apply Tikhonov for the majority of inversions, and high-pass Tikhonov only when it was necessary.

As suggested above, the angle searches using bipolar high-pass Tikhonov regularization (Figure 9.1) yielded the best indicators estimates of the proper orientation. The figures below demonstrate that the Summed Negative Values analysis is the best method to determine the proper orientation out of the sample for the bipolar case.

Figure 9.1 θ Search using High-Pass Tikhonov Regularization with White Noise

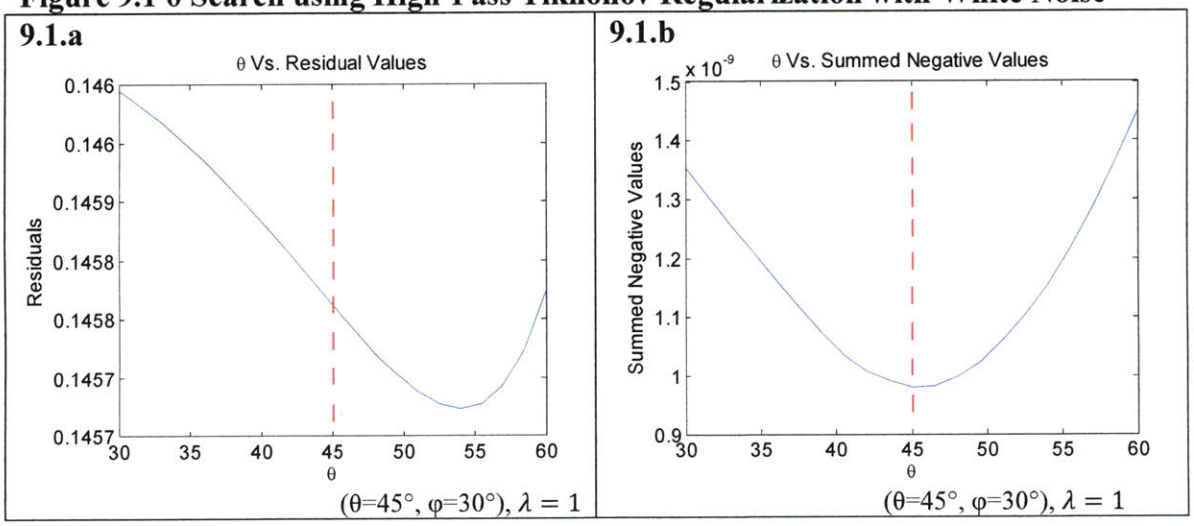

9.1.c

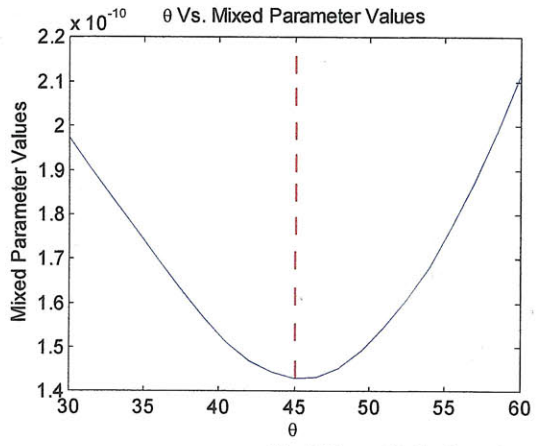

(θ=45°, φ=30°), $\lambda = 1$

9.1.d

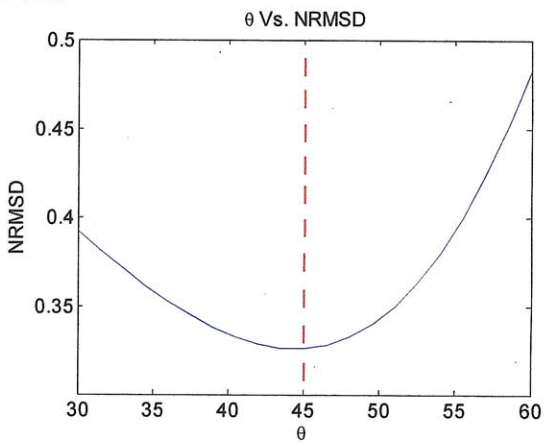

(θ=45°, φ=30°), $\lambda = 1$

The figures above demonstrate that high-pass Tikhonov Regularization is effective at searching for the proper orientation when white noise is added. The error indicators should have a minimum at $\theta = 45°$ (marked by the red dotted line) because the correct solution should yield the smallest amount of errors. Lambda is set to one for these scans because practice shows giving equal weight to the residual norm and the side constraint is an effective method for optimizing angles and height. λ cannot be properly optimized before knowing the orientation or height, so setting $\lambda = 1$ is a quick way to include Tikhonov regularization into the θ search. **9.1.a** is a plot of residual values of bipolar least squares method for a range of angles. **9.1.b** is a plot of summed negative values of bipolar least squares method for a range of angles. **9.1.c** is a plot of mixed parameter values of bipolar least squares method for a range of angles. **9.1.d** is a plot of NRMSD of bipolar least squares method for a range of angles.

Although the Tikhonov regularization methods applied in this study are succesful at estimating the orientation of a synthetic sample within a few degrees, they are not as effective at improving the estimates of the sample to sensor distance. The Tikhonov regularizations can provide a rough, order of magnitude estimation of the proper height, but these searches are not as accurate as their capability to determine the angular orientation of a sample's source distribution when higher levels of noise are present. The graph of height vs. NRMSD (9.2.d) has a desireable shape which indicates that the source distribution tends to be more accurate as simulations approach the proper height. However, such knowledge could not help determine the unknown height of a measurement as an ideal source distribution is a resource only available in synthetic data.

Figure 9.2 Height Searches using Bipolar High-Pass Tikhonov Regularization with White Noise

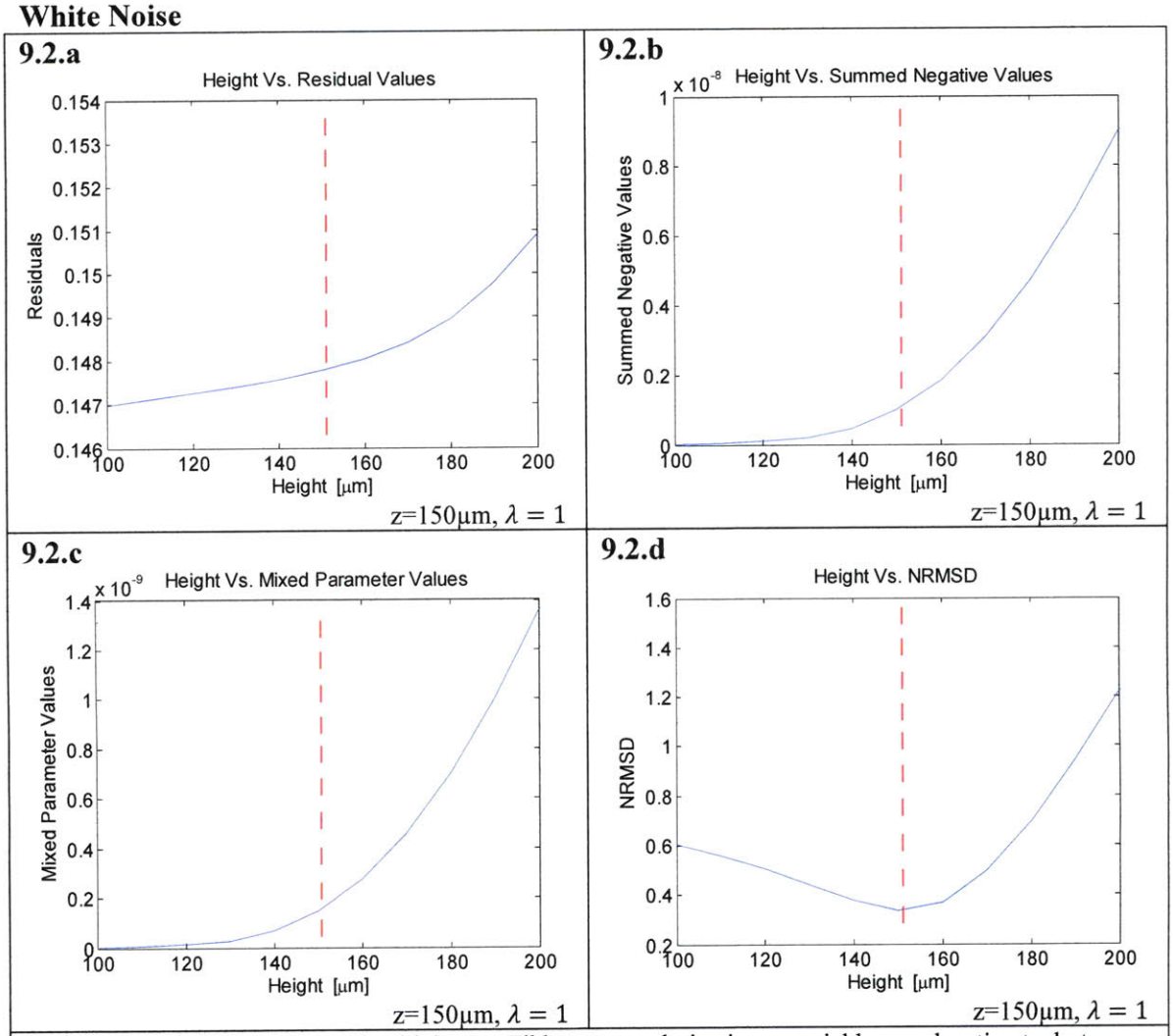

The figures above demonstrate that high-pass Tikhonov regularization can yield a rough estimate, but cannot provide a precise estimation of height through searching when white noise is added. The error indicators should have a minimum at z = 150 μm (marked by the red dotted line) because the correct solution should yield the smallest amount of errors. **9.2.a** is a plot of residual values of bipolar least squares method for a range of heights. **9.2.b** is a plot of summed negative values of bipolar least squares method for a range of heights. **9.2.c** is a plot of mixed parameter values of bipolar least squares method for a range of heights. **9.2.d** is a plot of NRMSD of bipolar least squares method for a range of heights. While the NRMSD plot has an accurate result, this technique is not applicable to real data with an unknown ideal source field.

After determining the correct orientation of the sample, and estimating the sample to sensor distance, better inversions can be obtained by optimizing λ. λ is optimized by finding the λ value on an L-curve where the residual norm and the solution norm find a balance (see Figure 9.3). The best value for λ will occur at the intersection of the two trends, where the solution norm and residual norm where the combination of the two values is at a minimum. In this case of high-pass Tikhonov regularization for the synthetic measurement with white noise added, $\lambda = .1$.

Figure 9.3 Determining Ideal Value for λ by L-Curve Analysis

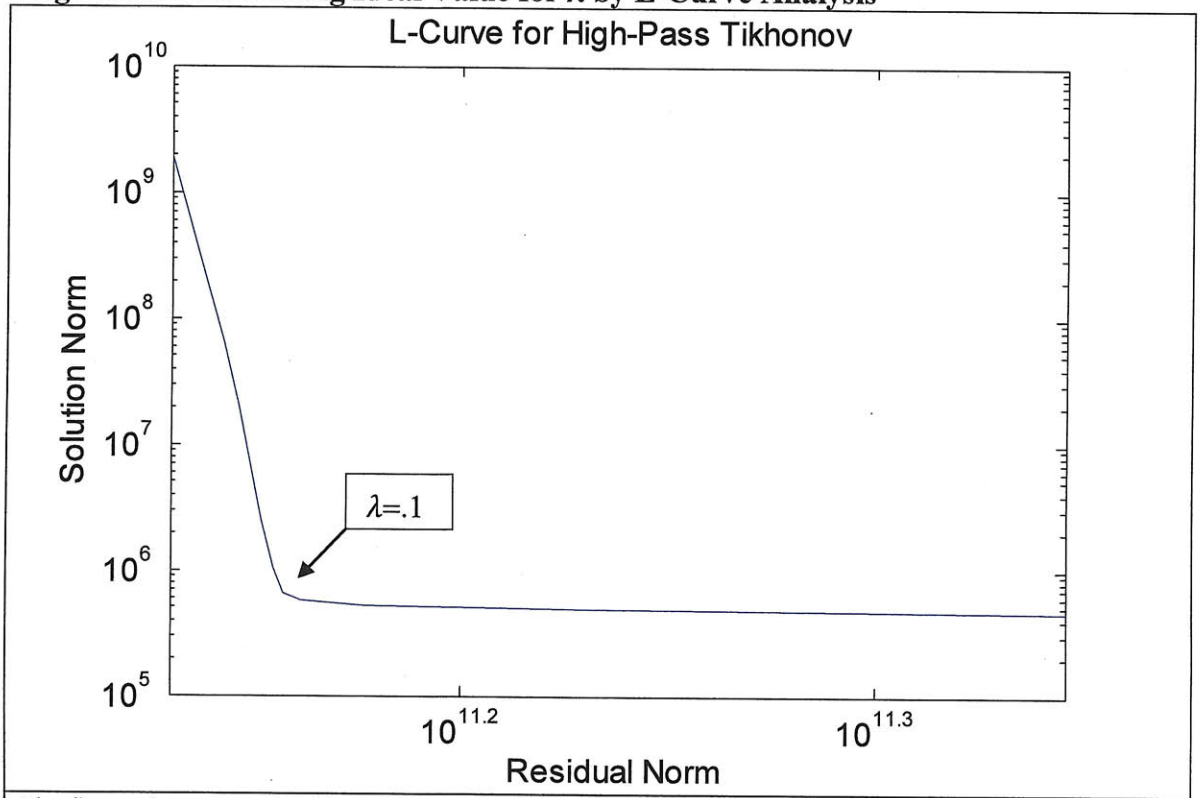

The figure above compares the solution norm to the residual norm on a log-log plot for a range of values of λ in order to determine the combined minimum of the two values. This minimum occurs at λ=1.

After determining the ideal value for λ through L-curve analysis, it is applied to inversions (see Figure 9.4).

Figure 9.4 Bipolar High-Pass Tikhonov Regularization with White Noise

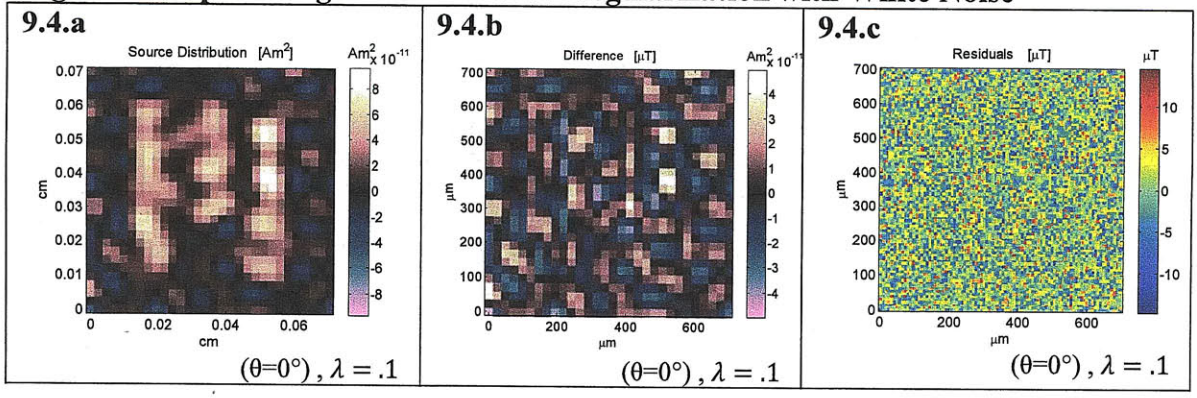

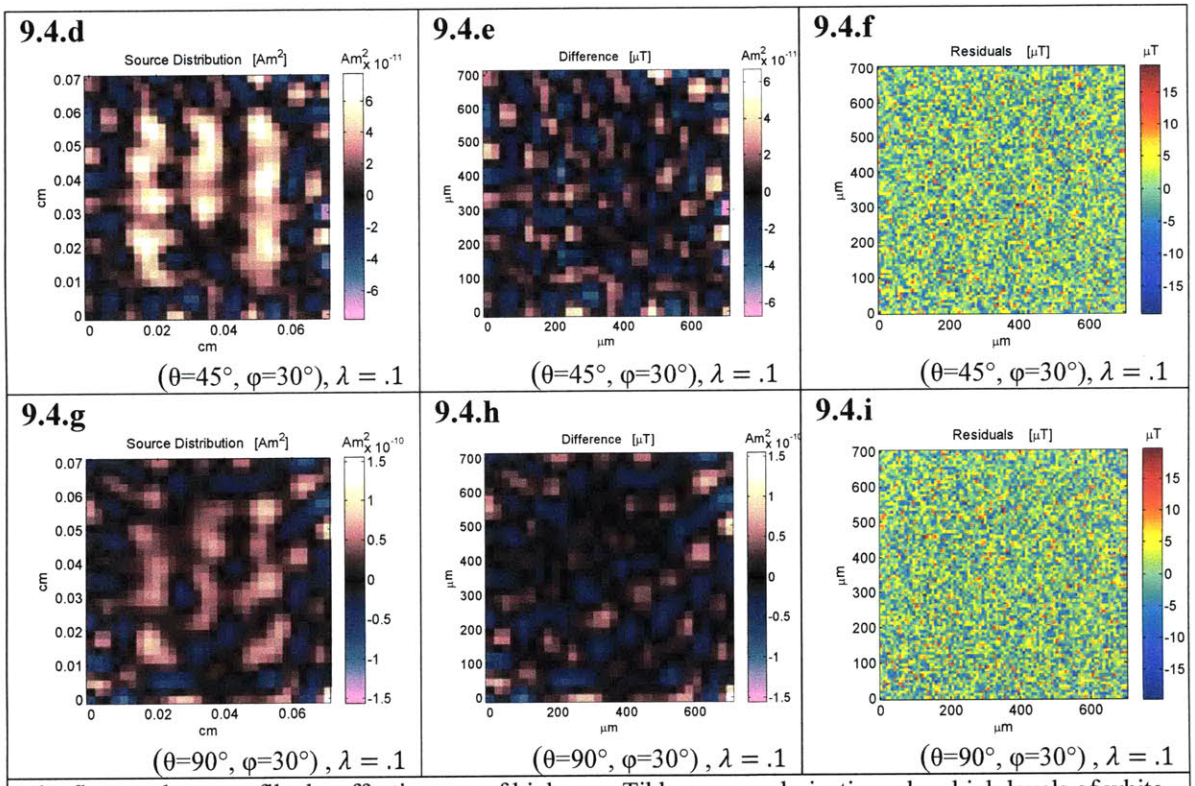

The figures above profile the effectiveness of high-pass Tikhonov regularization when high levels of white noise are present for three orientations. **9.4.a-b** For θ=0°, NRMSD=0.3269, Normalized Residual=0.1079, Summed Negative Values=8.9341×10^{-10}, Mixed Parameter Analysis=9.6392×10^{-11} **9.4.c-d** For θ=45°, φ=30°, NRMSD=0.3256, Normalized Residual=0.1473, Summed Negative Values=9.2106×10^{-10}, Mixed Parameter Analysis=1.3564×10^{-10} **9.4.e-f** For θ=90°, φ=30°, NRMSD= 0.3483, Normalized Residual= 0.1903, Summed Negative Values= 1.2088×10^{-9}, Mixed Parameter Analysis= 2.2998×10^{-10}

Hard TSVD θ searches performed similar to Tikhonov θ and height searches, although the minimum was less distinct. Hard TSVD inversions (Figure 10.1-4) took significantly longer to compute (high-pass Tikhonov is roughly 7.5 times faster than TSVD) and had slightly higher levels of error in comparison to Tikhonov regularization. Similar to how λ was determined for high-pass Tikhonov regularization, γ is determined by minimizing the combination of the solution norm and residual norm (see Figure 10.1). For the synthetic measurements with white noise added, the ideal value was optimized at approximately $\gamma = 100$.

Figure 10.1 Determining Ideal Value for γ by L-Curve Analysis

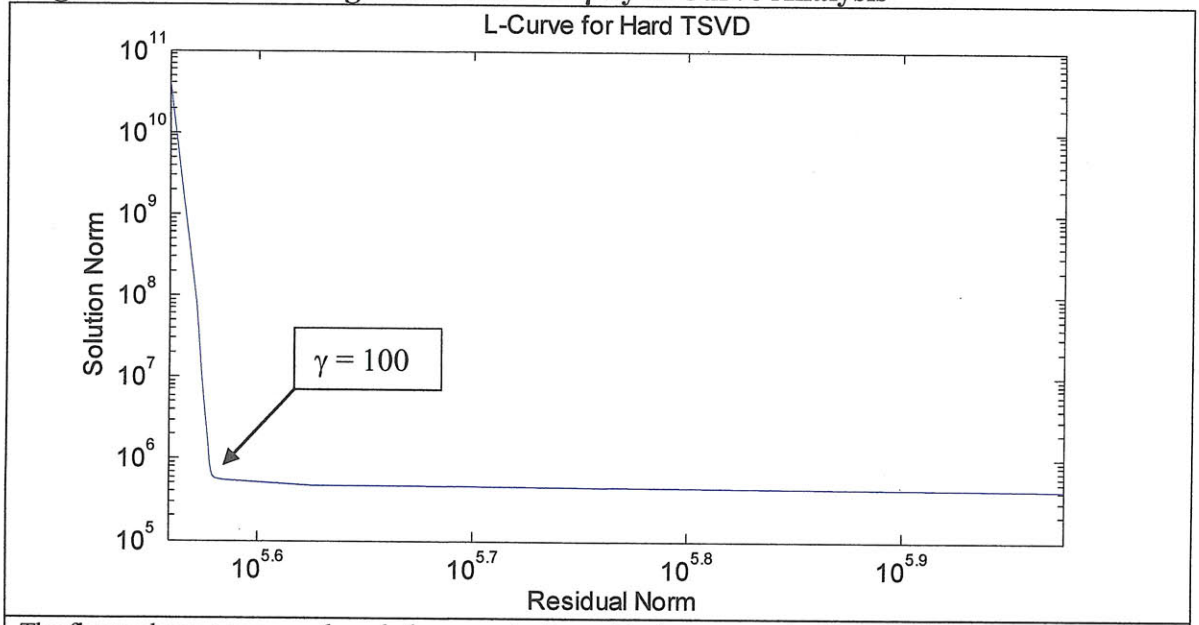

The figure above compares the solution norm to the residual norm on a log-log plot for a range of values of γ in order to determine the combined minimum of the two values. This minimum occurs at γ=100.

The optimized value for γ can be applied to the θ search (see Figure 10.2).

Figure 10.2 θ Searches using Bipolar Hard TSVD with White Noise

10.2.a

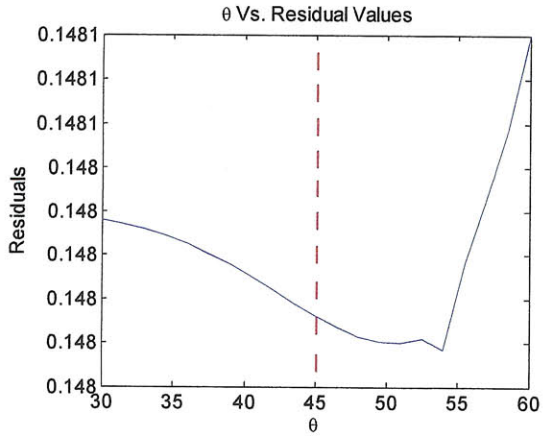

(θ=45°, φ=30°), γ = 100

10.2.b

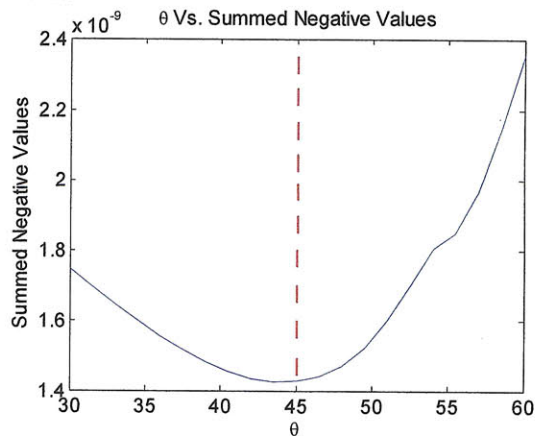

(θ=45°, φ=30°), γ = 100

10.2.c

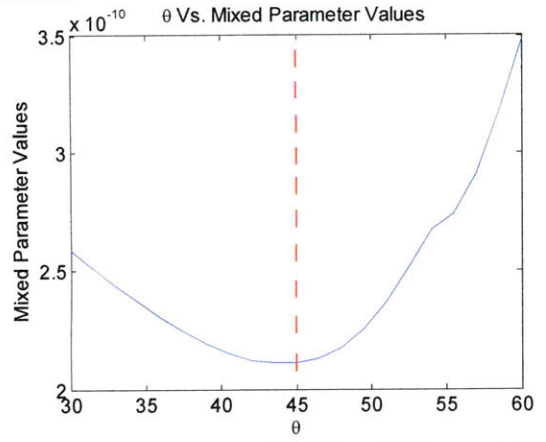

(θ=45°, φ=30°), $\gamma = 100$

10.2.d

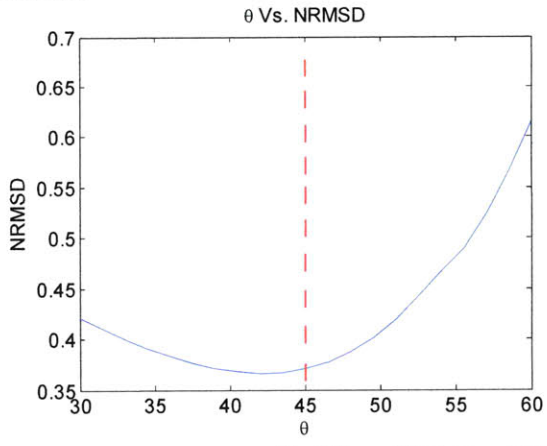

(θ=45°, φ=30°), $\gamma = 100$

The figures above demonstrates that TSVD is effective at searching for the proper orientation when white noise is added. The error indicators should have a minimum at θ = 45° (marked by the red dotted line) because the correct solution should yield the smallest amount of errors. **10.2.a** is a plot of residual values of bipolar least squares method for a range of angles. **10.2.b** is a plot of summed negative values of bipolar least squares method for a range of angles. **10.2.c** is a plot of mixed parameter values of bipolar least squares method for a range of angles. **10.2.d** is a plot of NRMSD of bipolar least squares method for a range of angles.

TSVD shares similar accuracy to high-pass Tikhonov regularization in its ability to search for the proper sample-to-sensor distance (see Figure 10.3).

Figure 10.3 Height Searches using Bipolar Hard TSVD with White Noise

10.3.a

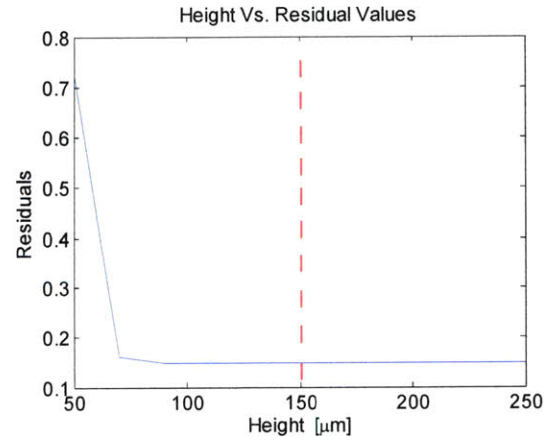

(z=150μm)

10.3.b

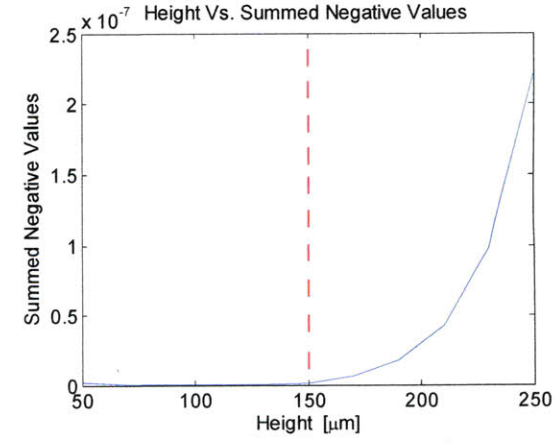

(z=150μm)

10.3.c

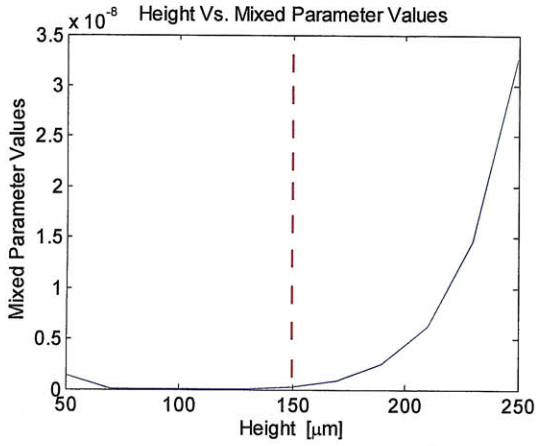

(z=150μm)

10.3.d

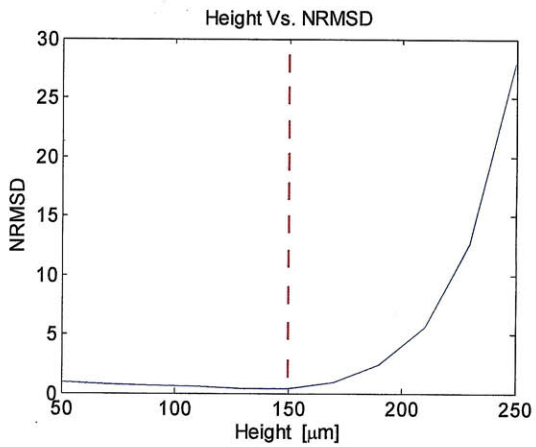

(z=150μm)

The figures above demonstrate that hard TSVD, like high-pass Tikhonov regularization can yield a rough estimate, but cannot provide a precise estimation of height through searching when white noise is added. The error indicators should have a minimum at z = 150 μm (marked by the red dotted line) because the correct solution should yield the smallest amount of errors. **10.3.a** is a plot of residual values of bipolar least squares method for a range of heights. **10.3.b** is a plot of summed negative values of bipolar least squares method for a range of heights. **10.3.c** is a plot of mixed parameter values of bipolar least squares method for a range of heights. **10.3.d** is a plot of NRMSD of bipolar least squares method for a range of heights. While the NRMSD plot has an accurate result, this technique is not applicable to real data with an unknown ideal source field.

When the orientation and proper height are known, TSVD performs at a similar level of accuracy in comparison to high-pass Tikhonov regularization (see Figure 10.4).

Figure 10.4 Bipolar Hard TSVD with White Noise

10.4.a

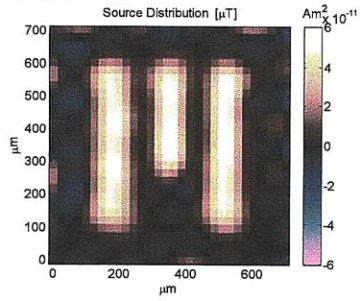

(θ=0°) γ =100

10.4.b

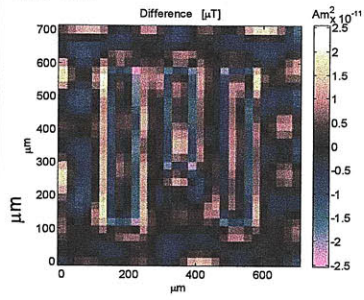

(θ=0°) γ =100

10.4.c

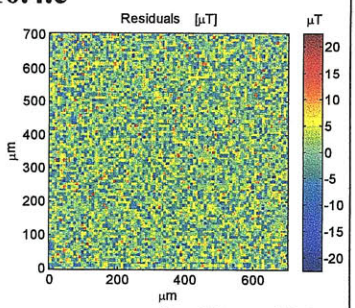

(θ=0°) γ =100

10.4.d

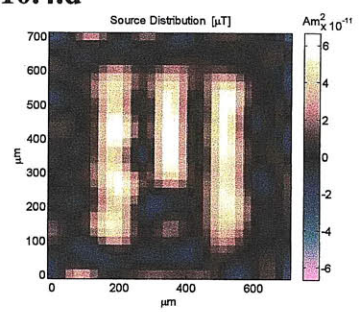

(θ=45°, φ=30°) γ =100

10.4.e

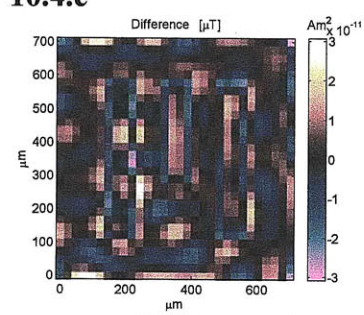

(θ=45°, φ=30°) γ =100

10.4.f

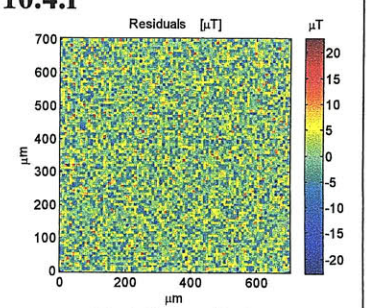

(θ=45°, φ=30°) γ =100

10.4.g

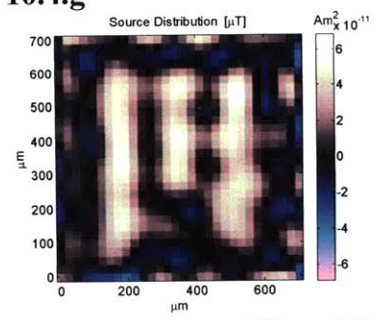

(θ=90°, φ=30°) γ =100

10.4.h

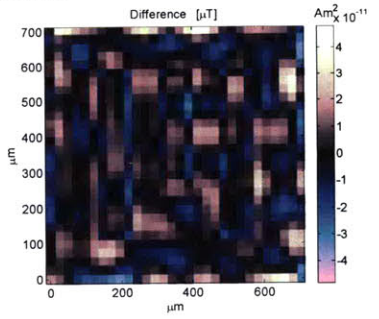

(θ=90°, φ=30) γ =100

10.4.i

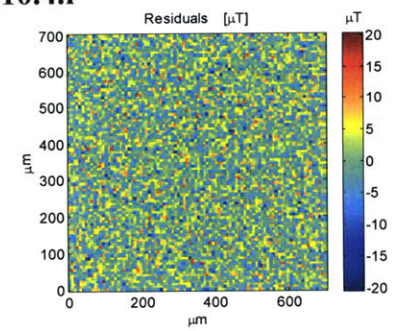

(θ=90°, φ=30°) γ =100

The figures above profile the effectiveness of hard TSVD when high levels of white noise are present for three orientations. Hard TSVD performs with similar accuracy as high-pass Tikhonov regularization. However, computation is 7.5 times slower. **10.4.a-b** For θ=0°, NRMSD=0.3210, Residual=0.1062, Summed Negative Values=1.2258×10^{-9}, Mixed Parameter Analysis=1.3022×10^{-10} **10.4.c-d** For θ=45°, φ=30°, NRMSD=0.3708 , Residual=0.1480, Summed Negative Values=1.4286×10^{-9}, Mixed Parameter Analysis=2.1146×10^{-10} **10.4.e-f** For θ=90°, φ=30°, NRMSD=0.5764, Residual=0.1924, Summed Negative Values=3.2887×10^{-9}, Mixed Parameter Analysis=6.3289×10^{-10}

In previous studies, three-component unipolar least squares method was shown to surpass 1-component unipolar least squares method (Lima & Weiss, 2009). However our investigation of three-component bipolar regularization techniques found no clear advantages to using three-component Tikhonov regularization (Figure 11.). It is important to note, three-component SVD could not be tested due to lack of memory available at our disposal (4GB and Windows XP 64 bits).

Figure 11.1 θ Searches using Bipolar Three-component Tikhonov Regularization with White Noise

11.1.a

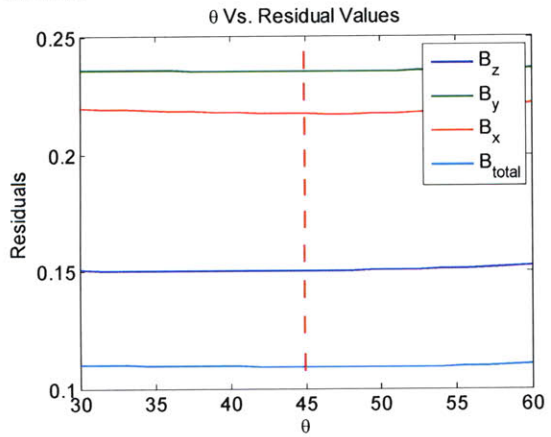

(θ=45°, φ=30°), $\lambda = 1$

11.1.b

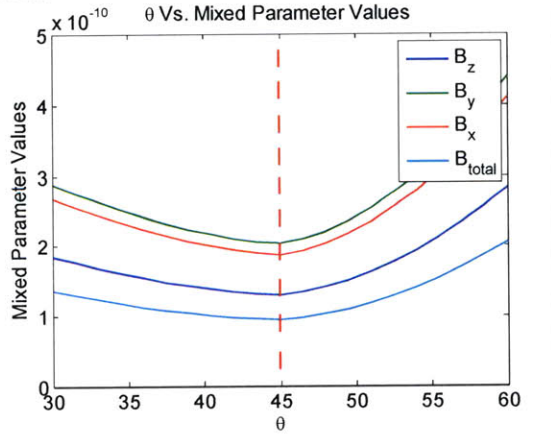

(θ=45°, φ=30°), $\lambda = 1$

11.1.c

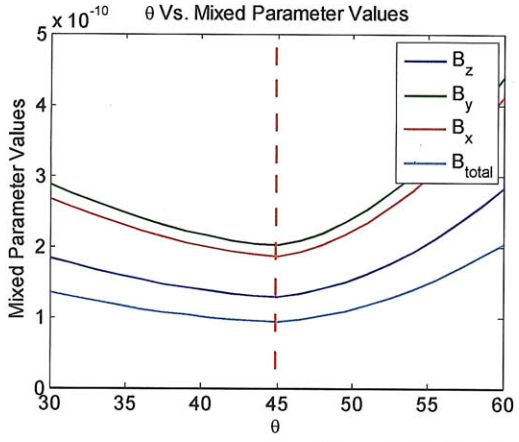

(θ=45°, φ=30°), $\lambda = 1$

11.1.d

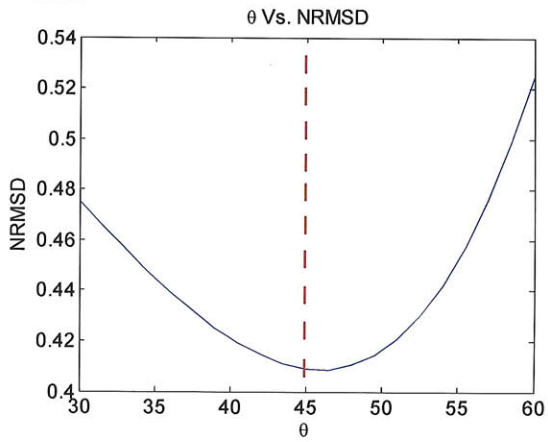

(θ=45°, φ=30°), $\lambda = 1$

The figures above demonstrates the effectiveness of bipolar three-component regularization at searching for the proper orientation when white noise is added. The error indicators should have a minimum at $\theta = 45°$ (marked by the red dotted line) because the correct solution should yield the smallest amount of errors. **11.1.a** is a plot of residual values of bipolar least squares method for a range of angles. **11.1.b** is a plot of summed negative values of bipolar least squares method for a range of angles. **11.1.c** is a plot of mixed parameter values of bipolar least squares method for a range of angles. **11.1.d** is a plot of NRMSD of bipolar least squares method for a range of angles.

Figure 11.2 Height Searches using Bipolar Three-component Tikhonov Regularization with White Noise

11.2.a

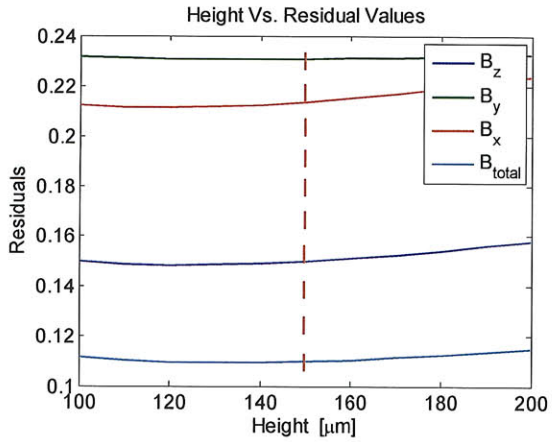

z=150μm, $\lambda = 1$

11.2.b

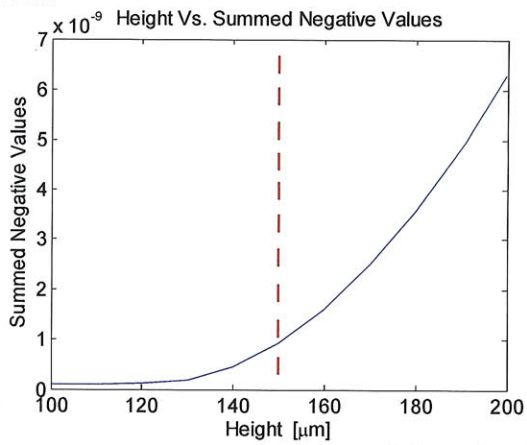

z=150μm, $\lambda = 1$

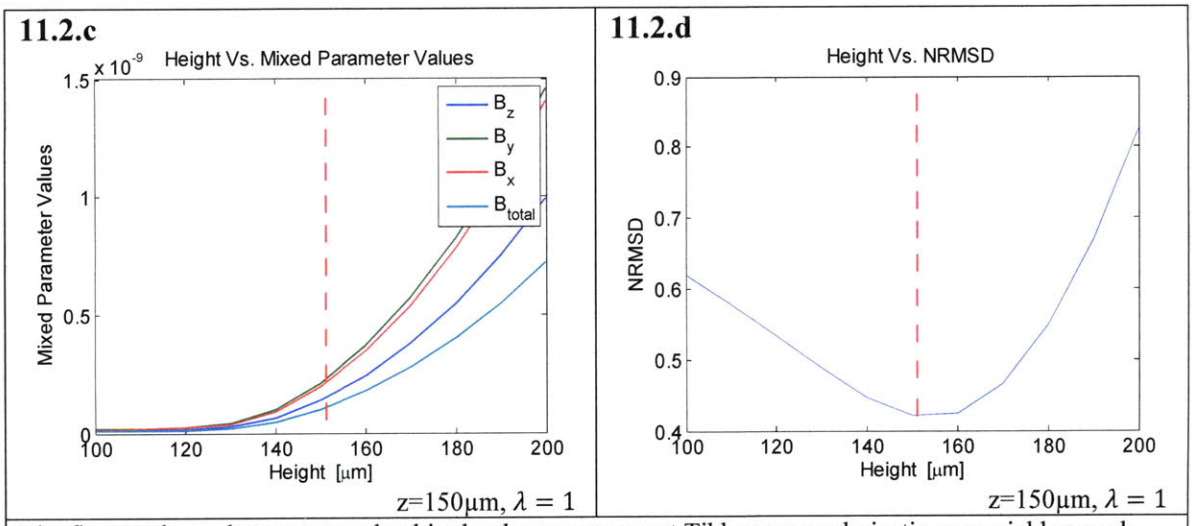

The figures above demonstrates that bipolar three-component Tikhonov regularization can yield a rough estimate, but cannot provide a precise estimation of height through searching when white noise is added. The error indicators should have a minimum at z = 150 μm (marked by the red dotted line) because the correct solution should yield the smallest amount of errors. **11.2.a** is a plot of residual values of bipolar least squares method for a range of heights. **11.2.b** is a plot of summed negative values of bipolar least squares method for a range of heights. **11.2.c** is a plot of mixed parameter values of bipolar least squares method for a range of heights. **11.2.d** is a plot of NRMSD of bipolar least squares method for a range of heights. While the NRMSD plot has an accurate result, this technique is not applicable to real data with an unknown ideal source field.

Using three-component analysis it is possible to measure the total strength of the measured field as well as the vertical z-component (see Figure 11.3).

Figure 11.3 Bipolar Three-component Tikhonov Regularization with White Noise

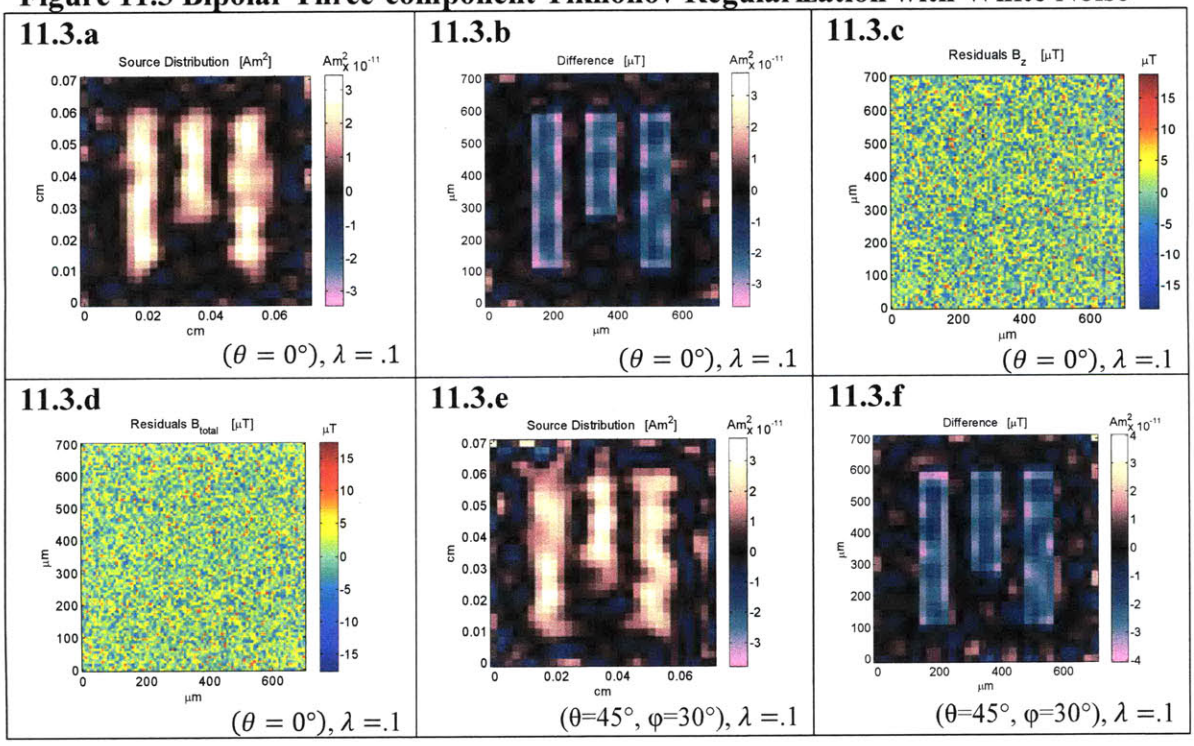

11.3.g

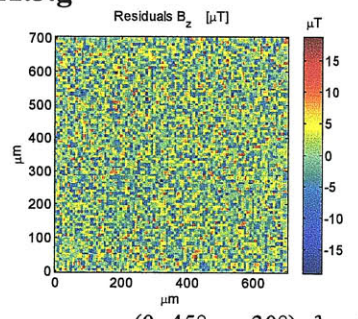

(θ=45°, φ=30°), λ =.1

11.3.h

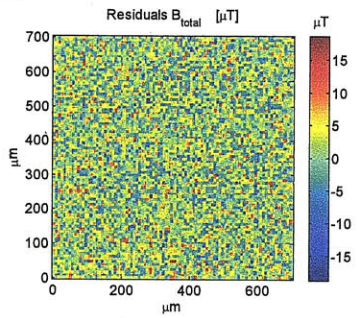

(θ=45°, φ=30°), λ =.1

11.3.i

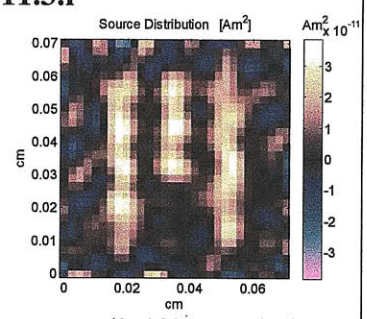

(θ=90°, φ=30°), λ =.1

11.3.j

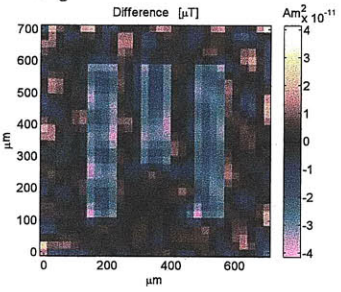

(θ=90°, φ=30°), λ =.1

11.3.k

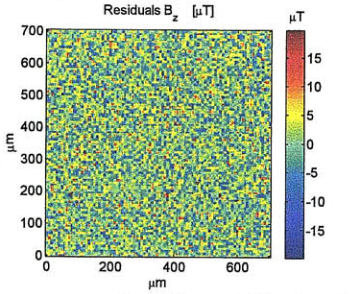

(θ=90°, φ=30°), λ =.1

11.3.l

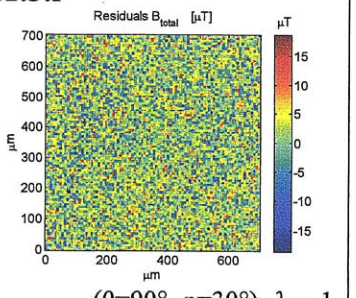

(θ=90°, φ=30°), λ =.1

The figures above profile the effectiveness of bipolar three-component Tikhonov when high levels of white noise are present for three orientations. Results are slightly worse than high-pass single-component Tikhonov regularization. Furthermore, three-component computaion is seven times slower than one component computation. **11.3.a-d** For θ=0°, NRMSD=0.4470, Residual: $B_z = 0.1062, B_y = 0.1578, B_x = 0.1579, B_{total} = 0.0765$, Summed Negative Values=2.0978×10^{-9}, Mixed Parameter Analysis: $B_z = 2.229 \times 10^{-10}, B_y = 3.311 \times 10^{-10}, B_x = 3.311 \times 10^{-10}$ $B_{total} = 1.606 \times 10^{-10}$ **11.3.e-h** For θ=45°, φ=30° NRMSD=0.5568, Residual: $B_z = 0.1474, B_y = 0.2309, B_x = 0.2121, B_{total} = 0.1069$, Summed Negative Values=2.8916×10^{-9}, 0.3090 Mixed Parameter Analysis: $B_z = 4.261 \times 10^{-10}, B_y = 6.676 \times 10^{-10}, B_x = 6.134 \times 10^{-10}, B_{total} = 3.090 \times 10^{-10}$ **11.3.i-l** For θ=90°, φ=30°, NRMSD=0.6719, Residual: $B_z = 0.1898, B_y = 0.3421, B_x = 0.2566, B_{total} = 0.1392$, Summed Negative Values=3.5874×10^{-9}, Mixed Parameter Analysis: $B_z = 6.81 \times 10^{-10}, B_y = 1.227 \times 10^{-9}, B_x = 9.20 \times 10^{-10}, B_{total} = 4.99 \times 10^{-10}$

Summary

In order to assess which methods are more effective, we have compared their computational time for a single inversion, height estimation ability, orientation estimation ability, NRMSD, normalized residuals, Summed Negative Values, and Mixed Parameter Analysis. The results are summarized in the table below.

Table 1 Bipolar Vs. Unipolar

Criteria:	Bipolar	Unipolar
Computational Time	11 seconds for Tikhonov regularization	254 seconds for Tikhonov regularization

<table>
<tr><td>Estimating Height</td><td>Both perform poorly at precise optimizations, yet can be used as rough indicators.</td><td>Both perform poorly at precise optimizations, yet can be used as rough indicators.</td></tr>
<tr><td>Estimating Orientation</td><td>Smoother optimization</td><td>More erratic optimization</td></tr>
<tr><td>NRMSD</td><td>Better (lower) with measurements that have lower quantities of noise and when TSVD or Tikhonov is applied

least squares inversions without noise:<table><tr><td>Orientation</td><td>NRMSD</td></tr><tr><td>θ=0°</td><td>0.0914</td></tr><tr><td>θ=45°, φ=30°</td><td>0.1631</td></tr><tr><td>θ=90°, φ=30°</td><td>0.8262</td></tr></table>
least squares inversions with noise (no regularization):<table><tr><td>Orientation</td><td>NRMSD</td></tr><tr><td>θ=0°</td><td>4.3355×10^{6}</td></tr><tr><td>θ=45°, φ=30°</td><td>$6.7293e\times 10^{6}$</td></tr><tr><td>θ=90°, φ=30°</td><td>1.4043×10^{7}</td></tr></table></td><td>Better (lower) with measurements that have higher quantities of noise. Also, can produce results from noisy data without TSVD or Tikhonov Regularization
least squares inversions without noise:<table><tr><td>Orientation</td><td>NRMSD</td></tr><tr><td>θ=0°</td><td>0.2984</td></tr><tr><td>θ=45°, φ=30°</td><td>0.2751</td></tr><tr><td>θ=90°, φ=30°</td><td>0.2667</td></tr></table>
least squares inversions with noise (no regularization):<table><tr><td>Orientation</td><td>NRMSD</td></tr><tr><td>θ=0°</td><td>.30071</td></tr><tr><td>θ=45°, φ=30°</td><td>.28452</td></tr><tr><td>θ=90°, φ=30°</td><td>.30235</td></tr></table></td></tr>
<tr><td>normalized residuals</td><td>Better (lower) with measurements that have lower quantities of noise

Least squares inversion without noise:<table><tr><td>Orientation</td><td>Normalized residuals</td></tr><tr><td>θ=0°</td><td>1.5840×10^{-8}</td></tr><tr><td>θ=45°, φ=30°</td><td>1.5416×10^{-8}</td></tr><tr><td>θ=90°, φ=30°</td><td>1.4718×10^{-8}</td></tr></table>
For least squares inversions with noise:<table><tr><td>Orientation</td><td>Normalized residuals</td></tr><tr><td>θ=0°</td><td>1.0256×10^{-1}</td></tr><tr><td>θ=45°, φ=30°</td><td>1.3853×10^{-1}</td></tr><tr><td>θ=90°, φ=30°</td><td>1.7832×10^{-1}</td></tr></table></td><td>Similar values with measurements that have higher quantities of noise
least squares inversions without noise:<table><tr><td>Orientation</td><td>Normalized residuals</td></tr><tr><td>θ=0°</td><td>1.7715×10^{-2}</td></tr><tr><td>θ=45°, φ=30°</td><td>1.5103×10^{-2}</td></tr><tr><td>θ=90°, φ=30°</td><td>1.0856×10^{-2}</td></tr></table>
For least squares inversions with noise:<table><tr><td>Orientation</td><td>Normalized residuals</td></tr><tr><td>θ=0°</td><td>1.0971×10^{-1}</td></tr><tr><td>θ=45°, φ=30°</td><td>1.4706×10^{-1}</td></tr><tr><td>θ=90°, φ=30°</td><td>1.9250×10^{-1}</td></tr></table></td></tr>
</table>

Summed Negative Values	Advantage: Has this additional indicator Disadvantage: Models dipole distribution with possible unrealistic negative values.	Advantage: Only models dipole distribution in the preferred orientation Disadvantage: Does not have this additional indicator
Mixed Parameter Analysis	Advantage: Has this additional indicator Disadvantage: Models dipole distribution with possible unrealistic negative values.	Advantage: Only models dipole distribution in the preferred orientation Disadvantage: Does not have this additional indicator

Our studies show that the bipolar method is better to use when computing inversions for magnetic microscopy maps with lower levels of noise. However, it can be advantageous to employ unipolar with noisy measurements.

Table 2. Tikhonov Vs. High-Pass Tikhonov

<table>
<tr><th>Criteria:</th><th>Tikhonov</th><th>Tikhonov High-Pass</th></tr>
<tr><td>Computational Time</td><td>13 seconds for bipolar regularization</td><td>15 seconds for bipolar regularization</td></tr>
<tr><td>Estimating Height</td><td>Very Similar</td><td>Very Similar</td></tr>
<tr><td>Estimating Orientation</td><td>Very Similar</td><td>Very Similar</td></tr>
<tr><td>NRMSD</td><td>Worse
<table><tr><th colspan="2">Bipolar with white noise:</th></tr><tr><td>Orientation</td><td>NRMSD</td></tr><tr><td>θ=0°</td><td>0.4082</td></tr><tr><td>θ=45°, φ=30°</td><td>0.5542</td></tr><tr><td>θ=90°, φ=30°</td><td>0.7433</td></tr></table></td><td>Better
<table><tr><th colspan="2">Bipolar with white noise:</th></tr><tr><td>Orientation</td><td>NRMSD</td></tr><tr><td>θ=0°</td><td>0.3269</td></tr><tr><td>θ=45°, φ=30°</td><td>0.3256</td></tr><tr><td>θ=90°, φ=30°</td><td>0.3483</td></tr></table></td></tr>
<tr><td>Normalized residuals</td><td>Worse (slightly larger)
<table><tr><th colspan="2">Bipolar with white noise:</th></tr><tr><td>Orientation</td><td>Normalized residuals</td></tr><tr><td>θ=0°</td><td>0.1079</td></tr><tr><td>θ=45°, φ=30°</td><td>0.1473</td></tr><tr><td>θ=90°, φ=30°</td><td>0.1903</td></tr></table></td><td>Better (slightly smaller)
<table><tr><th colspan="2">Bipolar with white noise:</th></tr><tr><td>Orientation</td><td>Normalized residuals</td></tr><tr><td>θ=0°</td><td>0.1065</td></tr><tr><td>θ=45°, φ=30°</td><td>0.1455</td></tr><tr><td>θ=90°, φ=30°</td><td>0.1899</td></tr></table></td></tr>
<tr><td>Summed Negative Values</td><td>Worse (slightly larger)
<table><tr><th colspan="2">Bipolar with white noise:</th></tr><tr><td>Orientation</td><td>Summed Negative Values</td></tr><tr><td>θ=0°</td><td>1.7715×10^{-9}</td></tr><tr><td>θ=45°, φ=30°</td><td>2.8109×10^{-9}</td></tr><tr><td>θ=90°, φ=30°</td><td>3.5229×10^{-9}</td></tr></table></td><td>Better (slightly smaller)
<table><tr><th colspan="2">Bipolar with white noise:</th></tr><tr><td>Orientation</td><td>Summed Negative Values</td></tr><tr><td>θ=0°</td><td>8.9341×10^{-10}</td></tr><tr><td>θ=45°, φ=30°</td><td>9.2106×10^{-10}</td></tr><tr><td>θ=90°, φ=30°</td><td>1.2088×10^{-9}</td></tr></table></td></tr>
<tr><td>Mixed Parameter</td><td>Worse</td><td>Better</td></tr>
</table>

Analysis	Bipolar with white noise:		Bipolar with white noise:	
	Orientation	Mixed Parameter Analysis	Orientation	Mixed Parameter Analysis
	$\theta=0°$	1.8867×10^{-10}	$\theta=0°$	9.6392×10^{-11}
	$\theta=45°, \varphi=30°$	4.0891×10^{-10}	$\theta=45°, \varphi=30°$	1.3564×10^{-10}
	$\theta=90°, \varphi=30°$	6.6905×10^{-10}	$\theta=90°, \varphi=30°$	6.6905×10^{-10}

This study found high-pass Tikhonov regularization to perform better quality inversions than identity matrix (minimum norm) Tikhonov regularization in NRMSD, normalized residuals, Summed Negative Values and Mixed Parameter Analysis. Neither method had a significant advantage in searching for the correct orientation and both performed similarly in determining height.

Table 3. Tikhonov Single-Component Vs. Tikhonov Three-Component

Criteria:	**Tikhonov 1-Component**	**Tikhonov 3-Component**
Computational Time	13 seconds for bipolar regularization	100 seconds for bipolar regularization
Estimating Height	Similar ability	Similar ability
Estimating Orientation	Similar ability	Similar ability
NRMSD	Better for $\theta=0°$ and $\theta=45°$, $\varphi=30°$	Better at $\theta=90°$, $\varphi=30°$
	Bipolar Tikhonov with white noise:	Bipolar Tikhonov with white noise:
	Orientation / NRMSD	Orientation / NRMSD
	$\theta=0°$ — 0.4082	$\theta=0°$ — 0.4470
	$\theta=45°, \varphi=30°$ — 0.5542	$\theta=45°, \varphi=30°$ — 0.5568
	$\theta=90°, \varphi=30°$ — 0.7433	$\theta=90°, \varphi=30°$ — 0.6719
Normalized residuals	Similar	Similar
	Bipolar Tikhonov with white noise:	Bipolar Tikhonov with white noise:
	Orientation / Normalized residuals	Orientation / Normalized residuals
	$\theta=0°$ — 0.1079	$\theta=0°$ — 0.1062
	$\theta=45°, \varphi=30°$ — 0.1473	$\theta=45°, \varphi=30°$ — 0.1474
	$\theta=90°, \varphi=30°$ — 0.1903	$\theta=90°, \varphi=30°$ — 0.1898

<table>
<tr><td>Summed Negative Values</td><td>Slightly better (lower)
<table><tr><th colspan="2">Bipolar Tikhonov with white noise:</th></tr><tr><td>Orientation</td><td>Summed Negative Values</td></tr><tr><td>θ=0°</td><td>1.7715×10^{-9}</td></tr><tr><td>θ=45°, φ=30°</td><td>2.8109×10^{-9}</td></tr><tr><td>θ=90°, φ=30°</td><td>3.5229×10^{-9}</td></tr></table></td><td>Slightly worse (higher)
<table><tr><th colspan="2">Bipolar Tikhonov with white noise:</th></tr><tr><td>Orientation</td><td>Summed Negative Values</td></tr><tr><td>θ=0°</td><td>2.0978×10^{-9}</td></tr><tr><td>θ=45°, φ=30°</td><td>2.8916×10^{-9}</td></tr><tr><td>θ=90°, φ=30°</td><td>3.5874×10^{-9}</td></tr></table></td></tr>
<tr><td>Mixed Parameter Analysis</td><td>Slightly better (lower)
<table><tr><th colspan="2">Bipolar with white noise:</th></tr><tr><td>Orientation</td><td>Mixed Parameter Analysis</td></tr><tr><td>θ=0°</td><td>1.8867×10^{-10}</td></tr><tr><td>θ=45°, φ=30°</td><td>4.0891×10^{-10}</td></tr><tr><td>θ=90°, φ=30°</td><td>6.6905×10^{-10}</td></tr></table></td><td>Slightly worse (higher)
<table><tr><th colspan="2">Bipolar with white noise:</th></tr><tr><td>Orientation</td><td>Mixed Parameter Analysis</td></tr><tr><td>θ=0°</td><td>2.229×10^{-10}</td></tr><tr><td>θ=45°, φ=30°</td><td>4.261×10^{-10}</td></tr><tr><td>θ=90°, φ=30°</td><td>6.81×10^{-10}</td></tr></table></td></tr>
</table>

This study suggests single-component Tikhonov regularization is superior to three-component regularization in producing lower or nearly equal values of NRMSD, normalized residuals, Summed Negative Values, and Mixed Parameter Analysis when λ is optimized to be 0.1 by the L-curve. Single-component also performs roughly 7.5 times faster than three-component Tikhonov.

Table 4. Hard Singular Value Decomposition Vs. Soft Singular Value Decomposition

<table>
<tr><th>Criteria:</th><th>TSVD Hard</th><th>TSVD Soft</th></tr>
<tr><td>Computational Time</td><td>95 seconds for bipolar regularization</td><td>77 seconds for bipolar regularization</td></tr>
<tr><td>Estimating Height</td><td>Better with noisy measurements</td><td>Worse with noisy measurements</td></tr>
<tr><td>Estimating Orientation</td><td>Better with noisy measurements</td><td>Worse with noisy measurements</td></tr>
<tr><td>NRMSD</td><td>Better with noisy measurements
<table><tr><th colspan="2">Bipolar white noise:</th></tr><tr><td>Orientation</td><td>NRMSD</td></tr><tr><td>θ=0°</td><td>0.3210</td></tr><tr><td>θ=45°, φ=30°</td><td>0.3708</td></tr><tr><td>θ=90°, φ=30°</td><td>0.5764</td></tr></table></td><td>Worse with noisy measurements
<table><tr><th colspan="2">Bipolar with white noise:</th></tr><tr><td>Orientation</td><td>NRMSD</td></tr><tr><td>θ=0°</td><td>0.4892</td></tr><tr><td>θ=45°, φ=30°</td><td>0.5415</td></tr><tr><td>θ=90°, φ=30°</td><td>0.6472</td></tr></table></td></tr>
<tr><td>Residuals</td><td>Better with noisy</td><td>Worse with noisy</td></tr>
</table>

<table>
<tr><td>Soft TSVD with white noise</td><td>measurements
<table><tr><th colspan="2">Bipolar with white noise:</th></tr><tr><td>Orientation</td><td>Normalized residuals</td></tr><tr><td>θ=0°</td><td>0.1062</td></tr><tr><td>θ=45°, φ=30°</td><td>0.1480</td></tr><tr><td>θ=90°, φ=30°</td><td>0.1924</td></tr></table></td><td>measurements
<table><tr><th colspan="2">Bipolar with white noise:</th></tr><tr><td>Orientation</td><td>Normalized residuals</td></tr><tr><td>θ=0°</td><td>0.1525</td></tr><tr><td>θ=45°, φ=30°</td><td>0.1858</td></tr><tr><td>θ=90°, φ=30°</td><td>0.2268</td></tr></table></td></tr>
<tr><td>Summed Negative Values
Hard TSVD with white noise</td><td>Better with noisy measurements
<table><tr><th colspan="2">Bipolar with white noise:</th></tr><tr><td>Orientation</td><td>Summed Negative Values</td></tr><tr><td>θ=0°</td><td>1.2258×10^{-9}</td></tr><tr><td>θ=45°, φ=30°</td><td>1.4286×10^{-9}</td></tr><tr><td>θ=90°, φ=30°</td><td>3.2887×10^{-9}</td></tr></table></td><td>Worse with noisy measurements
<table><tr><th colspan="2">Bipolar with white noise:</th></tr><tr><td>Orientation</td><td>Summed Negative Values</td></tr><tr><td>θ=0°</td><td>1.2488×10^{-10}</td></tr><tr><td>θ=45°, φ=30°</td><td>1.7582×10^{-9}</td></tr><tr><td>θ=90°, φ=30°</td><td>2.6805×10^{-9}</td></tr></table></td></tr>
<tr><td>Mixed Parameter Analysis</td><td>Better with noisy measurements
<table><tr><th colspan="2">Bipolar with white noise:</th></tr><tr><td>Orientation</td><td>Mixed Parameter Analysis</td></tr><tr><td>θ=0°</td><td>1.3022×10^{-10}</td></tr><tr><td>θ=45°, φ=30°</td><td>2.1146×10^{-10}</td></tr><tr><td>θ=90°, φ=30°</td><td>6.3289×10^{-10}</td></tr></table></td><td>Worse with noisy measurements
<table><tr><th colspan="2">Bipolar with white noise:</th></tr><tr><td>Orientation</td><td>Mixed Paraameter Analysis</td></tr><tr><td>θ=0°</td><td>1.9039×10^{-10}</td></tr><tr><td>θ=45°, φ=30°</td><td>3.2674×10^{-10}</td></tr><tr><td>θ=90°, φ=30°</td><td>6.0803×10^{-10}</td></tr></table></td></tr>
</table>

This study demonstrates that hard TSVD performs more accurate inversions than soft TSVD in terms of NRMSD, normalized residuals, Summed Negative Values, and Mixed Parameter Analysis.

Table 5. Tikhonov High-Pass Vs. Hard TSVD

Criteria:	**Tikhonov High-Pass**	**TSVD Hard**
Computational Time	15 seconds for bipolar regularization	95 seconds for bipolar regularization
Estimating Height	Similar	Similar
Estimating Orientation	Better	Worse

<table>
<tr>
<td>NRMSD</td>
<td>Better at θ=45°, φ=30° and θ=90°, φ=30° but slightly worse at θ=0°

Bipolar with white noise:
<table><tr><td>Orientation</td><td>NRMSD</td></tr><tr><td>θ=0°</td><td>0.3269</td></tr><tr><td>θ=45°, φ=30°</td><td>0.3256</td></tr><tr><td>θ=90°, φ=30°</td><td>0.3483</td></tr></table></td>
<td>Mixed, better at θ=0° but worse at at θ=45°, φ=30° and θ=90°, φ=30°

Bipolar with white noise:
<table><tr><td>Orientation</td><td>NRMSD</td></tr><tr><td>θ=0°</td><td>0.3210</td></tr><tr><td>θ=45°, φ=30°</td><td>0.3708</td></tr><tr><td>θ=90°, φ=30°</td><td>0.5764</td></tr></table></td>
</tr>
<tr>
<td>Residuals</td>
<td>Similar

Bipolar with white noise:
<table><tr><td>Orientation</td><td>Normalized residuals</td></tr><tr><td>θ=0°</td><td>0.1065</td></tr><tr><td>θ=45°, φ=30°</td><td>0.1455</td></tr><tr><td>θ=90°, φ=30°</td><td>0.1899</td></tr></table></td>
<td>Similar

Bipolar with white noise:
<table><tr><td>Orientation</td><td>Normalized residuals</td></tr><tr><td>θ=0°</td><td>0.1062</td></tr><tr><td>θ=45°, φ=30°</td><td>0.1480</td></tr><tr><td>θ=90°, φ=30°</td><td>0.1924</td></tr></table></td>
</tr>
<tr>
<td>Summed Negative Values</td>
<td>Better (slightly smaller)

Bipolar with white noise:
<table><tr><td>Orientation</td><td>Summed Negative Values</td></tr><tr><td>θ=0°</td><td>8.9341×10^{-10}</td></tr><tr><td>θ=45°, φ=30°</td><td>9.2106×10^{-10}</td></tr><tr><td>θ=90°, φ=30°</td><td>1.2088×10^{-9}</td></tr></table></td>
<td>Worse (slightly larger)

Bipolar with white noise:
<table><tr><td>Orientation</td><td>Summed Negative Values</td></tr><tr><td>θ=0°</td><td>1.2258×10^{-9}</td></tr><tr><td>θ=45°, φ=30°</td><td>1.4286×10^{-9}</td></tr><tr><td>θ=90°, φ=30°</td><td>3.2887×10^{-9}</td></tr></table></td>
</tr>
<tr>
<td>Mixed Parameter Analysis</td>
<td>Slightly better at θ=0° and θ=45°, φ=30° but slightly worse at θ=90°, φ=30°

Bipolar with white noise:
<table><tr><td>Orientation</td><td>Mixed Parameter Analysis</td></tr><tr><td>θ=0°</td><td>9.6392×10^{-11}</td></tr><tr><td>θ=45°, φ=30°</td><td>1.3564×10^{-10}</td></tr><tr><td>θ=90°, φ=30°</td><td>6.6905×10^{-10}</td></tr></table></td>
<td>Slightly better at θ=90°, φ=30° but slightly worse at θ=0° and θ=45°, φ=30°

Bipolar with white noise:
<table><tr><td>Orientation</td><td>Mixed Parameter Analysis</td></tr><tr><td>θ=0°</td><td>1.3022×10^{-10}</td></tr><tr><td>θ=45°, φ=30°</td><td>2.1146×10^{-10}</td></tr><tr><td>θ=90°, φ=30°</td><td>6.3289×10^{-10}</td></tr></table></td>
</tr>
</table>

In order to summarize how effective various methods are at determining proper orientation, the θ searches have been summarized in Figure 12.1 below. If not specified to be unipolar, assume the regularization technique is bipolar, and if not specified to be three-component, assume the regularization technique to be single-component.

Figure 12.1 Summary: θ Searches of Noisy Synthetic Measurements

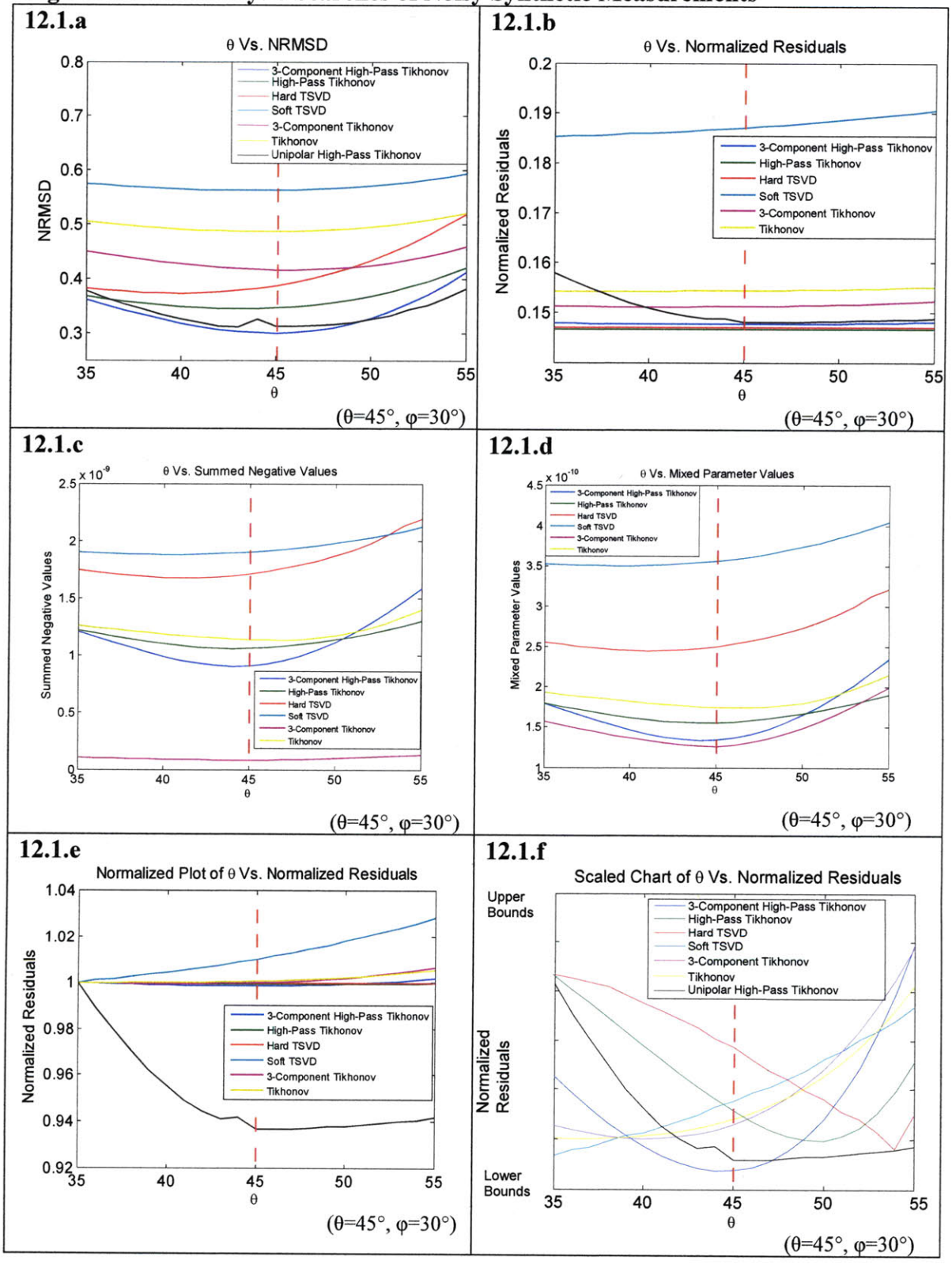

The Figures above describe the ability for various regularization methods to search for the proper orientation (θ=45°). For all Tikhonov regularization, λ=1. For hard TSVD, γ=100. For soft TSVD γ=0.1. It is important to note that results will vary depending on the regularization parameter value used. **12.1.a** Provides a comparison of various regularization methods in order to measure NRMSD Vs. θ. Listed from lowest to highest NRMSD values at θ=45°: (1.) 3-Component High-Pass Tikhonov (2.) Unipolar High-Pass Tikhonov (3.) High-Pass Tikhonov (4.) Hard TSVD (5.) 3-Component Tikhonov (6.)Tikhonov (7.) Soft TSVD **12.1.b** Provides a comparison of various regularization methods in order to measure normalized residuals vs. θ. Listed from lowest to highest normalized residuals at θ=45°: (1.) High-Pass Tikhonov (2.) Hard TSVD (3.) 3-component High-Pass Tikhonov (4.) Unipolar High-Pass Tikhonov (5.) 3-Component Tikhonov (6.) Tikhonov (7.) Soft TSVD **12.1.c** Provides a comparison of various regularization methods in order to measure Summed Negative Values vs. θ. Listed from lowest to highest Summed Negative Values at θ=45°: (1.) 3-Component High-Pass Tikhonov (2.) 3-Component High-Pass Tikhonov (3.) High-Pass Tikhonov (4.) Tikhonov (5.) Hard TSVD (6.) Soft TSVD **12.1.d** Provides a comparison of various regularization methods in order to measure Mixed Parameter Values vs. θ. Listed from lowest to highest Mixed Parameter Values at θ=45°: (1.) 3-Component High-Pass Tikhonov (2.) 3-Component High-Pass Tikhonov (3.) High-Pass Tikhonov (4.) Tikhonov (5.) Hard TSVD (6.) Soft TSVD **12.1.e** The Normalized Plot of a θ search is shown to demonstrate the variation Normalized Residuals relative to the Normalized Residual value at θ=35°. This graph demonstrates that unipolar High-Pass Tikhonov varies the most out off the methods tested relative to its original value. **12.1.f** Provides a scaled chart of normalized residuals vs. height. This plot displays the optimization curve shapes of various regularization methods in order to compare their ability to predict orientation through an absolute minimum of normalized residuals. To examine the actual values of these normalized residuals, refer to figure 12.1.b. 3-Component High-Pass Tikhonov appears to be the most effective at predicting the orientation by this method given the level of noise and the values of the regularization parameters (λ=1).

The data shown in Figure 12.1 above suggests that three-component high-pass Tikhonov is a superior method for searching for θ given the optimization constant values λ=1, hard TSVD γ=100, and soft TSVD γ=.1. An interesting phenomenon to note is that Tikhonov single-component has lower NRMSD than three-component when λ is set to 0.1 by L-curve optimization, if the orientation and height are previously known. However, when λ is set to equal 1 to simulate a standard θ search, three-component Tikhonov high-pass regularization out-perform all other methods tested in NRMSD search as well as displaying the best normalized residual θ search shape demonstrated on the scaled chart of normalized residuals. Furthermore, 3-component high-pass Tikhonov manages to have the second lowest values for Summed Negative Values as well as Mixed Parameter Values in addition to a minimum at the proper orientation of θ=45°.

In order to summarize how effective various methods are at determining proper sample-to-sensor distance, height searches have been summarized in Figure 12.2 below. If not specified to be unipolar, assume the regularization technique is bipolar, and if not specified to be three-component, assume the regularization technique to be single-component.

Figure 12.2 Summary: Height Searches of Noisy Synthetic Measurements

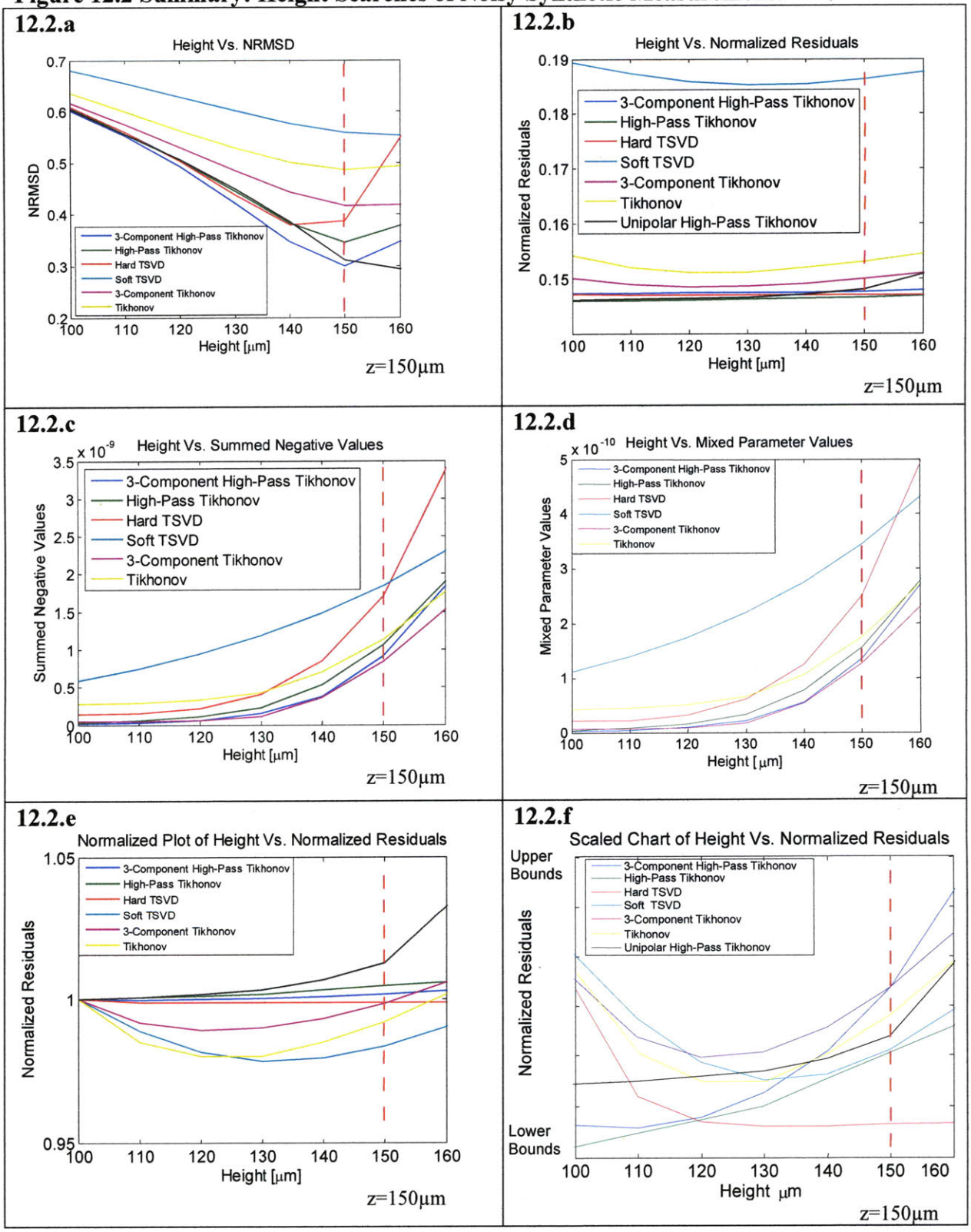

The Figures above describe the ability for various regularization methods to search for the proper height. For all Tikhonov regularization, λ=1. For hard TSVD, γ=100. For soft TSVD γ=0.1. It is important to note that results will vary depending on the regularization parameter value used. **12.2.a** Provides a comparison of various regularization methods in order to measure NRMSD vs. height. Three-component high-pass Tikhonov regularization has the lowest value out of the metrics examined as well as having one of the most clearly defined minimums. **12.2.b** Provides a comparison of various regularization methods in order to measure normalized residuals vs. height. **12.2.c** Provides a comparison of various regularization methods in order to measure Summed Negative Values vs. height. **12.2.d** Provides a comparison of various regularization methods in order to measure Mixed Parameter Values vs. height. **12.2.e** The Normalized Plot of a θ search is shown to demonstrate the variation Normalized Residuals relative to the Normalized Residual value at θ=35°. This graph demonstrates that unipolar High-Pass Tikhonov varies the most out off the methods tested relative to its original value. **12.2.f** Provides a scaled chart of normalized residuals vs. height. This plot displays the optimization curve shape of various regularization methods in order to compare their ability to predict orientation through an absolute minimum of normalized residuals.

Our study of height search found no method evaluated could accurately measure the height of the sample. However, some could roughly approximate the height within 20 μm. Out of the methods shown in Figure 12.2, single-component high-pass Tikhonov is the suggested method to search for height because it is fast, has one of the lowest values of NRMSD when λ=1 and the lowest when λ is optimized. It doesn't perform significantly better than other methods, but it also does not perform significantly worse.

Our study found that aside from θ searches where three-component Tikhonov High-Pass is the preferred method, single-component Tikhonov High-Pass is the most favorable regularization technique to employ because it is fast and performs better at the metrics chosen for this study. Therefore, we will apply this regularization technique to the real samples. On the other hand, when testing different values for the regularization parameter, SVD is much faster, as it does not require decomposing the matrix multiple times.

Real Measurements:

The magnetization within the shocked basalt was oriented in the vertical direction θ=0°. We used single-component high-pass Tikhonov to confirm the sample's known orientation of $\theta = 0°$ and sample-to-sensor distance of 610μm. As the synthetic data suggested, the Tikhonov high-pass solution was a good indicator of the proper orientation, but a less adequate indicator of height. The normalized residuals were low (0.0187). And qualitatively, the source distribution had a form that closely matched the shape of the sample. Because the measurement had high levels of noise, unipolar inversions yielded lower normalized residuals than bipolar inversions.

Figure 13.1 Shocked Basalt: θ Search Using High-Pass Tikhonov

13.1.a

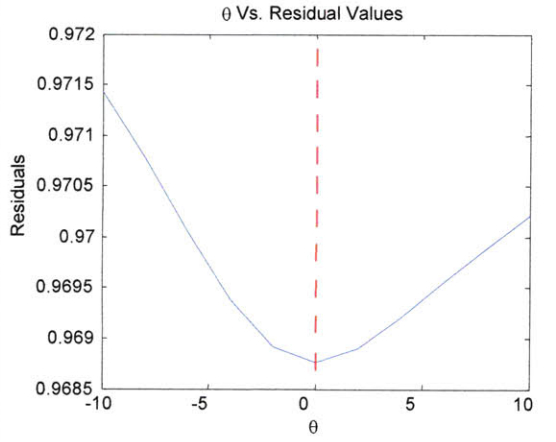

$(\theta=0°), \lambda = 1$

13.1.b

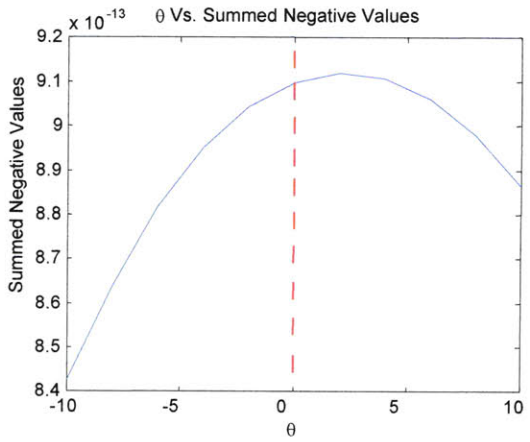

$(\theta=0°), \lambda = 1$

13.1.c

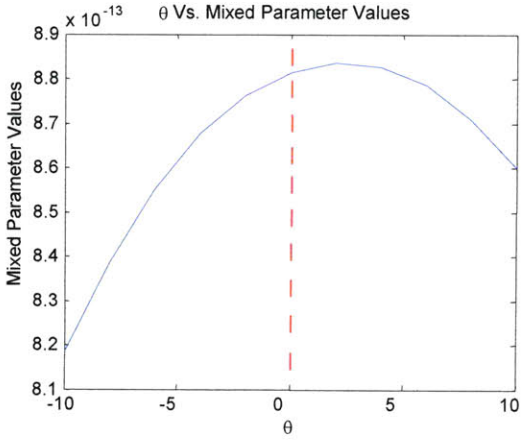

$(\theta=0°), \lambda = 1$

The figures above document a θ search of a shocked basalt with a known orientation at θ=0°. **13.1.a** normalized residuals of the shocked basalt inversion with respect to θ **13.1.b** Summed Negative Values with respect to θ **13.1.b** Mixed Parameter Values with respect to θ. The red dotted line marks where a previous study meausred the orientation to be.

Synthetic data analysis earlier in this study suggested that Summed Negative Values (Figure 13.1.b) and Mixed Parameter Values (Figure 13.1.c) are better indicators of orientation than residuals (Figure 13.1.a). However, these sample data suggest the reverse. Future studies should understand that both methods can be employed as rough indicators, but neither normalized residual nor Summed Negative Values nor Mixed Parameter Analysis can claim to be precise measurements of the correct orientation of noisy data. Often qualitative analysis can be an effective tool for finding better solutions in real data where there is no known ideal source field to check results with. Often misleading results can be identified by stray dipoles that are present outside where the sample is located. Not only did past studies (Gattacceca, Boustie, Lima, Weiss, de Resseguier, & Cuq-Lelandais, 2010) suggest the orientation was θ=0°, but quantitative analysis of the source distribution at various angles confirmed that in this example, normalized residuals was a better indicator than Summed Negative Values and Mixed Parameter Analysis.

The sample to sensor distance was recorded in a previous study (Gattacceca, Boustie, Lima, Weiss, de Resseguier, & Cuq-Lelandais, 2010) to be 610 μm. Knowing this, it was possible to assess the acuracy of the height search (Figure 13.2)

Figure 13.2 Shocked Basalt: Height Search Using Bipolar High-Pass Tikhonov

13.2.a

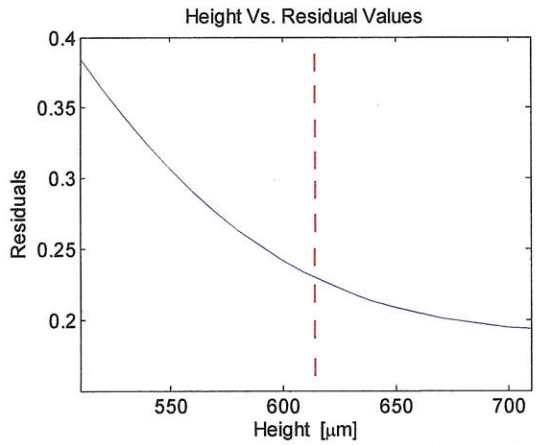

z=610μm, $\lambda = 1$

13.2.b

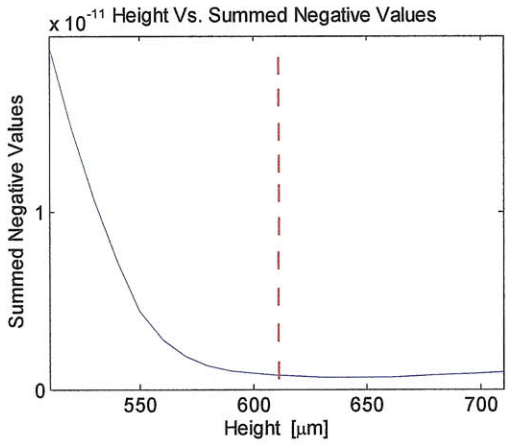

z=610μm, $\lambda = 1$

13.2.c

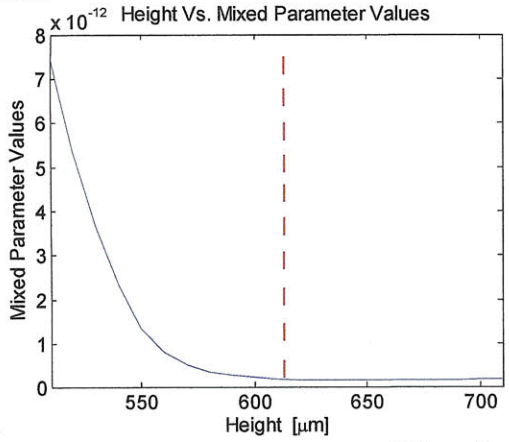

z=610μm, $\lambda = 1$

13.2a-c The figures above demonstrate the effectiveness of bipolar high-pass Tikhonov regularization to determine the sample—to—sensor distance on a real sample. Summed Negative Values and Mixed Parameter Analysis are more effective at this analysis than examining the residual values.

As demonstrated on synthetic data, normalized residuals, Summed Negative Values and Mixed Parameter Values are imprecise indicators of height. Similar to the orientation analysis, the quantitative results of the inversion searches provided rough indicators of proper values that could then be investigated qualitatively results that appear closer to the real value.

Knowing the height and orientation, it is possible to invert the shocked basalt (see figure 13.3 below)

Figure 13.3 Shocked Basalt: Inversion obtained with Unipolar High-Pass Tikhonov Regularization

13.3.a

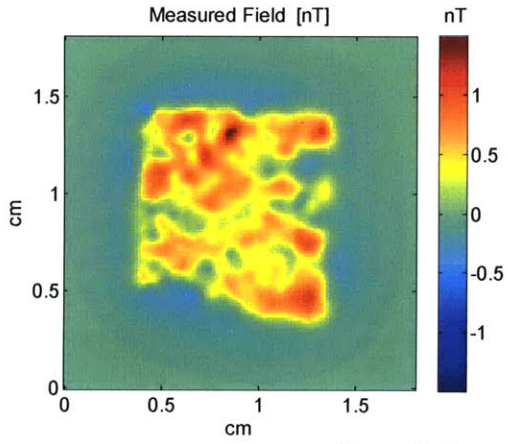

$(\theta = 0°), \lambda = 10^{-5}$

13.3.b

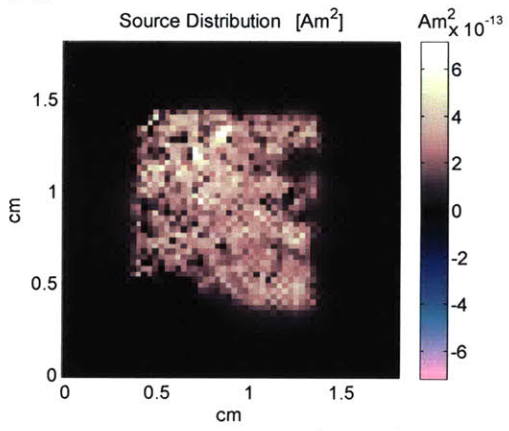

$(\theta = 0°), \lambda = 10^{-5}$

13.3.c

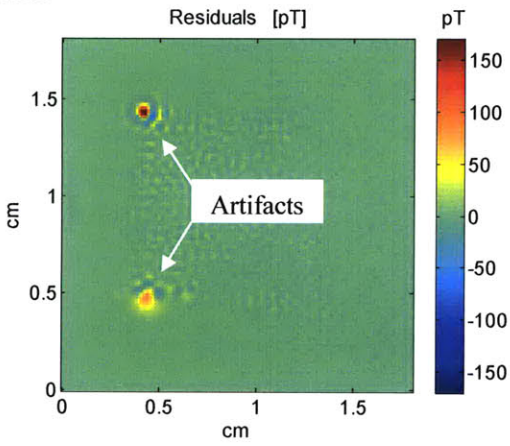

$(\theta = 0°), \lambda = 10^{-5}$

The above figures describe the measurement and inversion analysis of the shocked basalt **13.3.a** SQUID microscope measurement of the shocked basalt. **13.3.b** Source distribution of the shocked basalt. **13.3.c** Residual map of the shocked basalt. normalised residuals=0.0187. The artifacts present in the residuals are most likely caused by non-unidirectional components present due to contamination or sample damage during the preparation process.

The refrigerator magnet was measured with a Magnetic Instrumentation Inc. hall sensing teslameter Model 2100. Our setup placed the outermost tip of the teslameter 3 mm above the sample, but the location of the actual sensor within the instrument could not be precisely identified by the manual or by a company technician. The direction of the magnetization of the sample was not known beforehand. Our analysis yielded estimates for the orientation and sample-to-sensor distance of (θ =100°, φ =88°), and 7 mm, respectively.

Figure 14.1 Refrigerator Magnet: θ Search Using Three-Component High-Pass Tikhonov

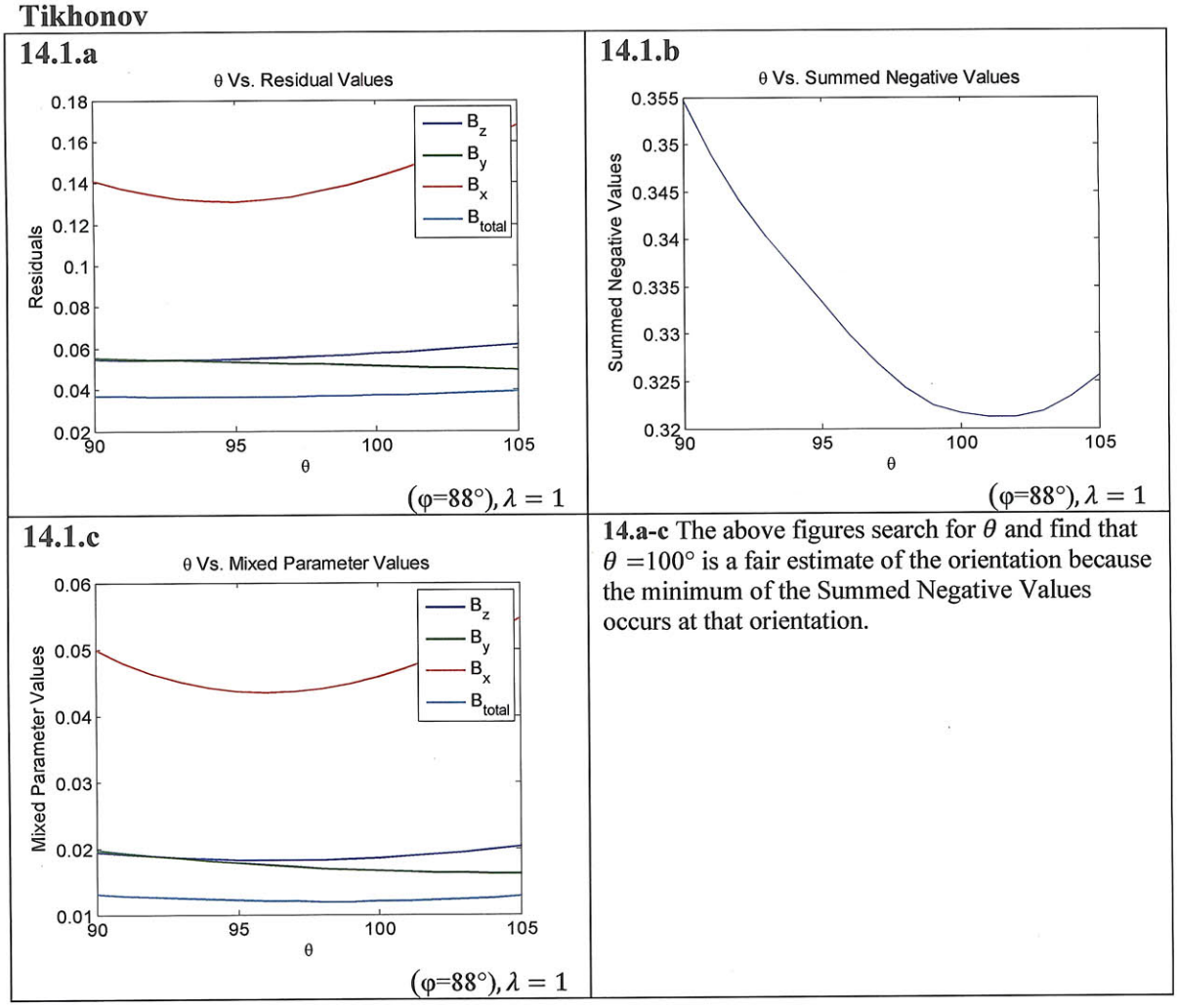

14.a-c The above figures search for θ and find that θ =100° is a fair estimate of the orientation because the minimum of the Summed Negative Values occurs at that orientation.

Figure 14.1 above graphs a variety of indicators in order to search for θ. Along with examining normalized residuals, Summed Negative Values and Mixed Parameter Analysis, we qualitatively examined source distributions and found that the best combination of quantitative indicators and qualitative realistic looking source distributions occurred around θ =100°.

After determining the proper orientation of the sample, the height could be determined by searching for minimums in normalized residuals, Summed Negative Values, and Mixed Parameter Analysis along with qualitative analysis of source distribution maps (Figure 14.2). Although there is no ideal source distribution to check the results of this inversion, it has normalized residuals as low as 0.0296. It also has a very convincing residual map that posseses a random distribution of residuals. Still it is important to note the small artifacts marring the source distribution image, revealing that the orientation and height used to calculate the inversion are still not exactly precise.

Figure 14.2 Refrigerator Magnet: Height Search Using Bipolar High-Pass Tikhonov

14.2.a

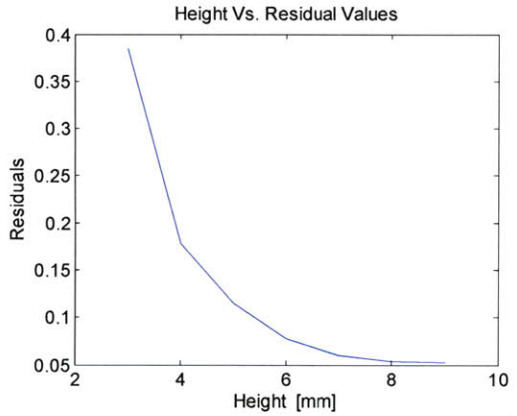

$\lambda = 1$

14.2.b

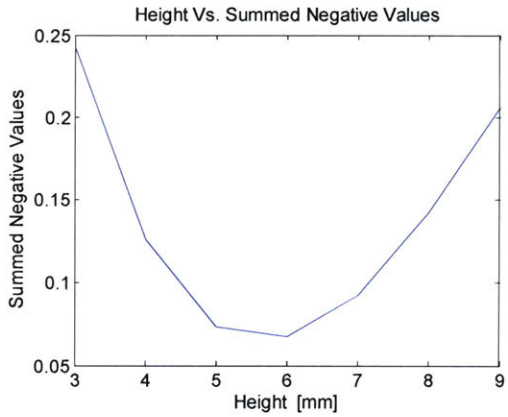

$\lambda = 1$

14.2.c

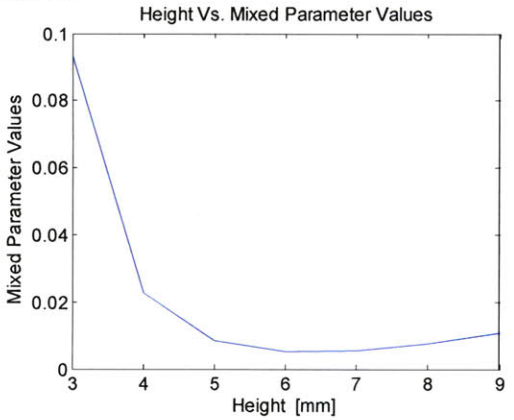

$\lambda = 1$

The figures above search for the sample-to-sensor distance employing various error indicators. **14.a** normalized residuals with respect to height **14.b** Summed Negative Values with respect to height **14.c** Mixed Parameter Values with respect to height. Mixed Parameter analysis indicates that the distance is 7 mm.

In Figure 14.2 (above), Mixed Parameter Values have a defined minimum around 7 mm, suggesting that the sample-to-sensor is distance is roughly 7 mm. This argument is strengthened by qualitativly realistic source distribution map that is generated when inversions are applied at that height.

For the refrigerator magnet, bipolar inversions had lower residuals than unipolar inversions because of the low levels of noise in the magnetic measurement. This is demonstrated in Figure 14.3 (below).

Figure 14.3 Refrigerator Magnet: Inversion obtained with Bipolar High-Pass Tikhonov Regularization

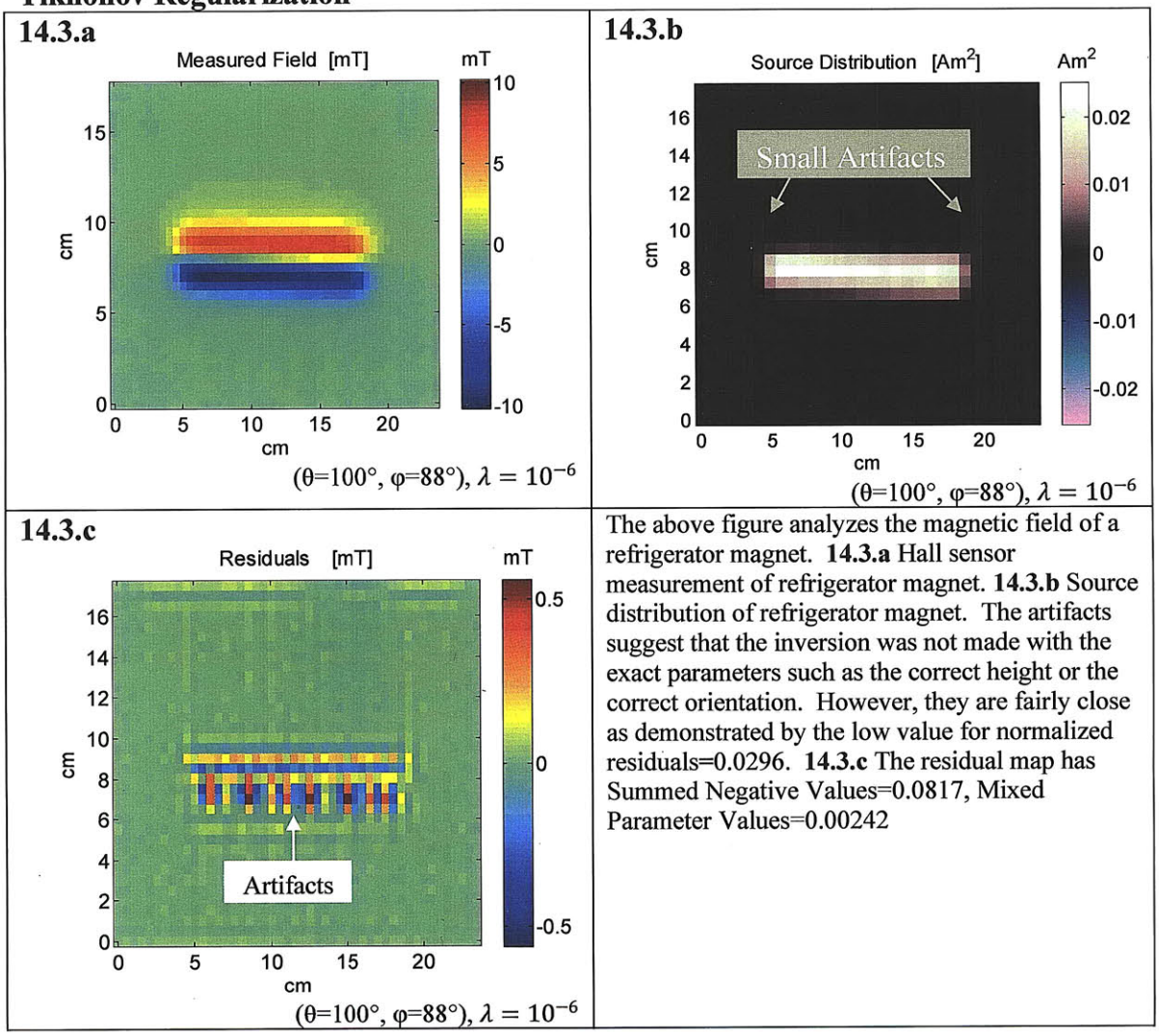

The above figure analyzes the magnetic field of a refrigerator magnet. **14.3.a** Hall sensor measurement of refrigerator magnet. **14.3.b** Source distribution of refrigerator magnet. The artifacts suggest that the inversion was not made with the exact parameters such as the correct height or the correct orientation. However, they are fairly close as demonstrated by the low value for normalized residuals=0.0296. **14.3.c** The residual map has Summed Negative Values=0.0817, Mixed Parameter Values=0.00242

9. Conclusion

In this study we analyzed different methods for retrieving information about the magnetization distribution within planar samples from magnetic field maps measured with scanning microscopes. In particular, we evaluated the effectiveness of bipolar and unipolar constraints on the source distribution, and found that bipolar performs better with measurements that have lower levels of noise, while unipolar performs equally well or better with higher levels of noise. This trend persists in all types of regularization tested. In normalized least squares inversions of synthetic data, bipolar is superior when no noise was added (for θ=0°, NRMSD is 0.0914 for bipolar and 0.2984 for unipolar) , but when noise was added, bipolar failed while unipolar continued to function (for θ=0°, NRMSD is 4.3355×10^6 for bipolar and for unipolar .30071). Through our analysis of unregularized least for bipolar squares method, Tikhonov regularization, Tikhonov regularization with a high-pass filter, TSVD soft and TSVD hard, we found that single-component Tikhonov regularization with a high-pass filter matrix was usually the most effective method of analysis. An exception to this trend was that three-component high-

pass Tikhonov proves superior in θ searches when we added noise to the sample and set λ=1. However, three-component Tikhonov regularization and high-pass Tikhonov regularization take more time to compute and for most analysis do not have a significant advantage over single-component Tikhonov regularization. After finding the best methods for our purposes, we applied unipolar Tikhonov regularization with a high-pass filter to a real SM magnetic field map of a shocked basalt with a known magnetization orientation and an estimated sample-to-sensor distance. Our methods could accurately predict the angle and could provide a rough estimate of the height. Our optimized inversion of the field map yielded normalized residuals= 0.0187. We also applied high-pass Tikhonov regularization to the inversion of experimental field maps of a refrigerator magnet. Because of the low levels of noise it was advantageous to use bipolar models in this case. The magnetization orientation was unknown as well as the sample to sensor distance. We estimated the orientation at $\theta = 100°$, $\varphi = 88°$and a sample-to-sensor distance of 7 mm. A strong indication that these might be the right values is the fact that the bipolar high-pass Tikhonov regularization worked very well: normalized residuals=0.0296, Summed Negative Values=0.0817, Mixed Parameter Analysis=0.00242.

10. Acknowledgements:
This project would not have been possible without the outstanding instruction and guidance of Dr. Eduardo Lima. His deep understanding of electromagnetism physics and SQUID technology along with his talent for educating others profoundly increased the efficiency of my work. Thanks must as well be awarded to Professor Benjamin Weiss for his fundamental contributions to this paper along with his planetary science lectures which inspired my initial interest in paleomagnetism. Jane Connor and Professor Kamal Youcef-Toumi were also of great importance in ensuring I effectively communicated my findings. I also must thank Jérôme Gattacecca (CEREGE, France) for providing the sample of the shocked basalt.

References

Brearley, A.J. (2003) Nebular vs parent body processing of chondritic meteorites. In '*Treatise on Geochemistry*' , Cosmochemistry Vol. 1. Editors Holland and Turekian. Elsevier. *pp. 711. ISBN 0-08-043751-6. Elsevier, 2003., p.247-268.*

Butler, R. F. (2004, September). *PALEOMAGNETISM: Magnetic Domains to Geological Terranes.* Retrieved April 10, 2010, from PALEOMAGNETISM: Magnetic Domains to Geological Terranes Electronic Edition, September 2004: http://www.pmc.ucsc.edu/~njarboe/pmagresource/ButlerPaleomagnetismBook.pdf

Clarke, J., & Braginski, A. I. (2004). *The Squid Handbook Vol. 1.* Weinheim, Germany: Wiley-VCH.

Clarke, J., & Braginski, A. I. (2006). *The SQUID Handbook, Vol. 2.* Weinheim, Germany: Wiley.

Gattacceca, J., Berthe, L., Boustie, M., Vadeboin, F., Rochette, P., & de Resseguier, T. (2008). On the efficiency of shock magnetization processes. *Phys. Earth Planet Interiors 166* , 1-10.

Gattacceca, J., Boustie, M., Lima, E., Weiss, B. P., de Resseguier, T., & Cuq-Lelandais, J. P. (2010) *Physics of the Earth and Planetary Ineriors*, Submitted. Unraveling the simultaneous shock magnetization and demagnetization of rocks.

Hansen, P. C. (1994). Regularization tools: a Matlab package for analysis and solution of discrete ill-posed problems. *Numerical Algorithms 6* , 1-35.

Jenks, W. G., Thomas, I. M., & Wikswo, J. P. (1997). SQUIDS. *Encyclopedia of Applied Physics, Vol. 19* , 457-468.

Krot, A. N., Hutcheon, I. D., Brearley, A. J., Pravdivtseva, O. V., Petaev, M. I., & Hohenberg, C. M. (2005). Timescales and Settings for Alteration of Chrondritic Meteorites. In *Meteorites and Early Solar System II* (pp. 525-553).

Krot, A. N., Scott, E. R., & Zolensky, M. E. (1995). Mineralogical and chemical modification of components in CV3 chondrites: Nebular or asteroidal processing? *Meteoritics* , 748-775.

Lima, E. A., & Weiss, B. P. (2009). Obtaining Vector Magnetic Field Maps from Single-Component Measurements of Geological Samples. *Journal of Geophysical Research-Solid Earth* , Vol. 114, B06102, doi:10.1029/2008JB006006, 2009.

Scott, E. R., & Krot, A. N. (2007). In *Chondrites and Their Components* (pp. 1-72). Honolulu, HI.

Weiss, B. P., Fong, L. E., Vali, H., Lima, E. A., & Baudenbacher, F. J. (2008). Paleointensity of the Ancient Martian magnetic field. *Geophysical Research Letters* Vol. 35, L23207, 5 PP., 2008 doi:10.1029/2008GL035585 .

Weiss, B. P., Lima, E. A., Fong, L. E., & Baudenbacher, F. J. (2007). Paleomagnetic analysis using SQUID microscopy. *Journal of Geophysical Research Vol. 112* , B09105, 20 PP., 2007doi:10.1029/2007JB004940